Supporting Information for

Electronic Insights into Aminoquinoline-Based PN^{H}N Ligands: Protonation State Dictates Geometry While Coordination Environment Dictates Acidity and N-H Bond Strength

Matthew V. Gradiski‡, Benjamin Rennie‡, Alan J. Lough, and Robert H. Morris*

Davenport Chemical Research Laboratories, Department of Chemistry, University of Toronto 80
St. George Street , Toronto, Ontario, Canada, M5S 3H6

1. Synthesis and discussion of nickel complex **4**……………………………………………........S2
2. NMR spectra of reported complexes and pK_a studies………………………………………….S4
3. pK_a calculations……………………………………………………………………………….S13
4. UV-Vis spectra & Beer-Lambert plots……………………………………………………..S15
5. DFT calculated molecular orbitals…………………………………………………………….S21
6. Cyclic voltammograms and BDFE calculations……………………………………………S23
7. EPR spectrum of proposed Fe(III) complex………………………………………………..S25
8. XRD structure of **5(BF$_4$)** molecule B…………………………………………………….S26
9. NMR spectra of attempted synthesis of an amido complex of 7…………………………...S27
10. Crystal data and structure refinement……………………………………………………...S28

Synthesis and Discussion of Nickel Complex 4.

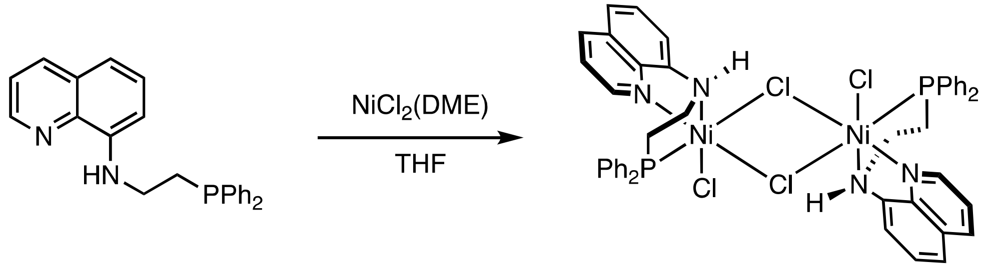

L1^{H} (**4**) 76%

Scheme S1. Synthesis of dimeric nickel complex 4.

Rather than the desired 4-coordinate square planar cationic complex, an octahedral chloride bridged dimeric complex analogous to that of our previously reported dimeric iron complex[1] $[FeCl_2(L^H)]_2$ is obtained as a lime green powder. Single crystal XRD of **4** (Figure S1; top) reveals the dimeric structure and the *fac* coordination geometry of the ligand. The green solid experiences a colour change when dissolved in dry MeOH and changes colour to ruby red. When the MeOH solvent is removed under vacuum or the solid is precipitated or crystallized from methanol by addition of pentane or other suitable hydrocarbon, the colour changes back to green and the dimeric species is isolated. We postulate that the red species in solution is monomeric and MeOH aids in the disruption and breaking of the dimeric structure. All efforts in attempting to isolate a red solid from a MeOH solution of **4** were unsuccessful and even slow evaporation resulted in the reappearance of the green dimeric species. Minor evidence for the disruption of the dimeric structure by MeOH is found via the solid-state structure of **4** in which co-crystallized MeOH solvent molecules experience significant hydrogen bonding with the apical non-bridging chloride ligand (Figure S1; bottom). The measured $d(\mathrm{OH}\cdots\mathrm{Cl})$ hydrogen bonding is 2.31(2) Å while the N–H functionality hydrogen bonds to the same chloride ligand with a measured $d(\mathrm{NH}\cdots\mathrm{Cl(1)})$ of 2.72(3) Å and a bridging chloride ligand of distance $d(\mathrm{NH}\cdots\mathrm{Cl(2)})$ 2.77(2) Å. It is possible that when complex **4** is placed in a MeOH rich environment the hydrogen bonding is sufficient enough within the network to force the bridging chloride ligands into a single donor that experiences similar hydrogen bonding from MeOH as Cl(1) does as shown in Figure S1. If the dimeric structure breaks, a coordination site would be left vacant in which a solvent molecule could coordinate to occupy. Under these conditions, a 6-coordinate octahedral structure is likely more stable than a 5-coordinate TBP structure. Nonetheless, the red species is paramagnetic as evidenced by its silent $^{31}P\{^1H\}$ NMR spectrum and broadened and paramagnetically shifted ^1H NMR spectrum when **4** is dissolved in CD_3OD (Figure S7). The solvent coordination bond is relatively weak as evidenced by the occurrence of re-dimerization when the complex is removed from the MeOH environment via crystallization or when placed under vacuum.

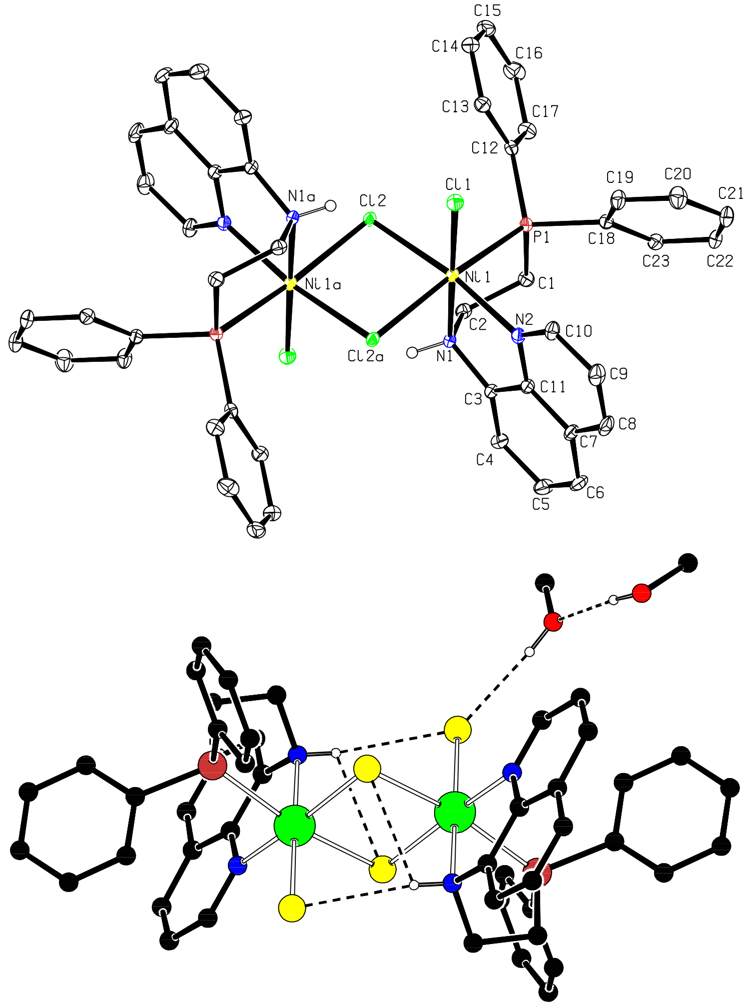

Figure S1. X-ray diffraction-derived structure of 4 with co-crystallized MeOH solvent molecules removed (top). Ball-and-stick structure of 4 showing close contact hydrogen bonding (bottom). Ellipsoids are shown at 30% probability. Carbon-bound hydrogen atoms have been omitted for clarity.

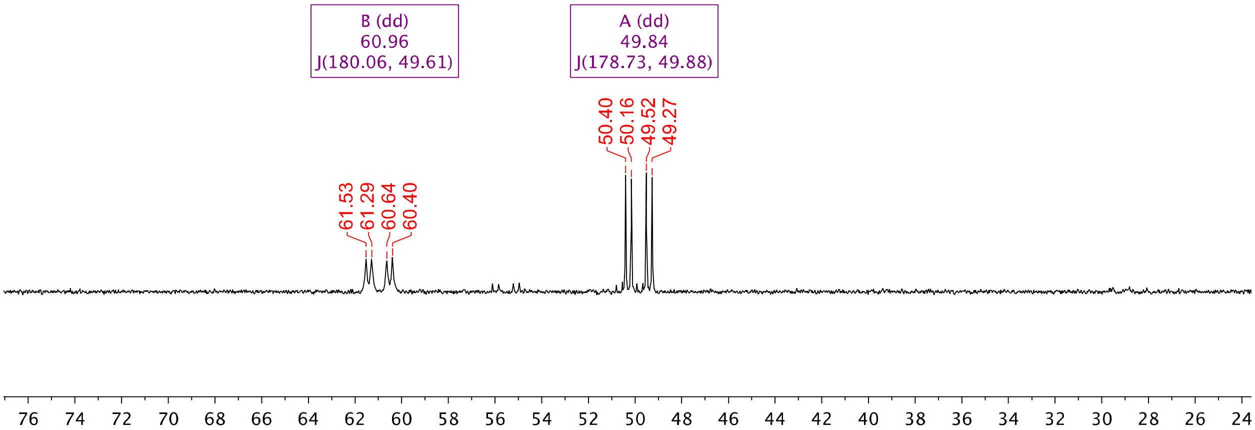

Figure S2. $^{31}P\{^1H\}$ **NMR spectrum (202 MHz,** CD_2Cl_2**) of 1.**

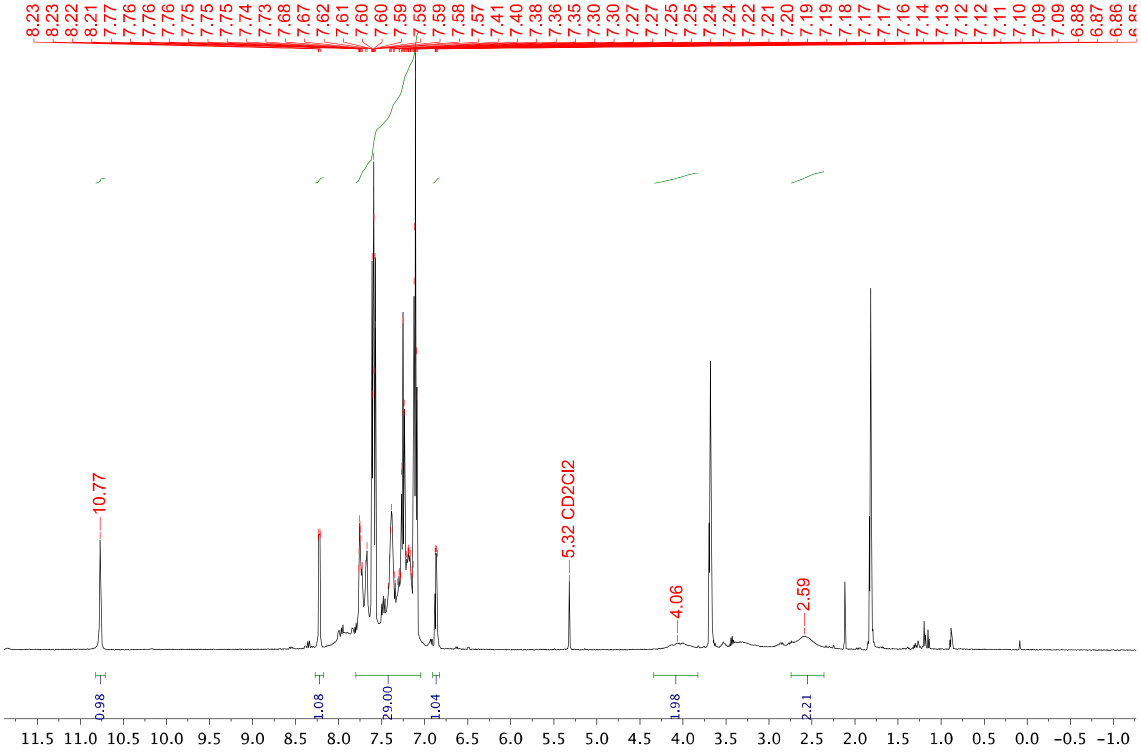

Figure S3. ^1H **NMR spectrum (500 MHz,** CD_2Cl_2**) of 1.**

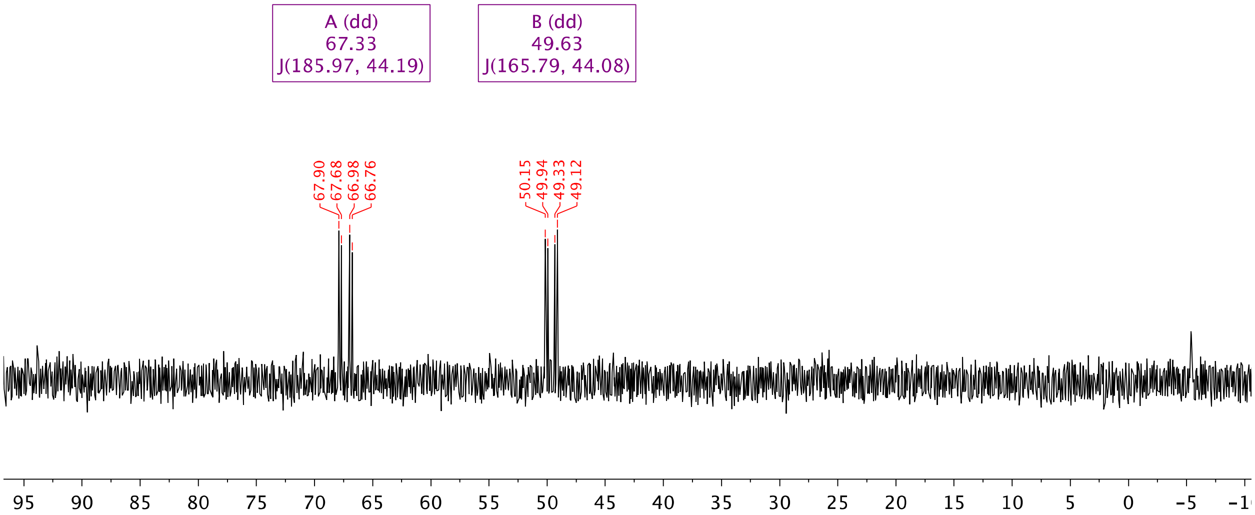

Figure S4. $^{31}P\{^1H\}$ **NMR spectrum (202 MHz,** C_6D_6**) of 2.**

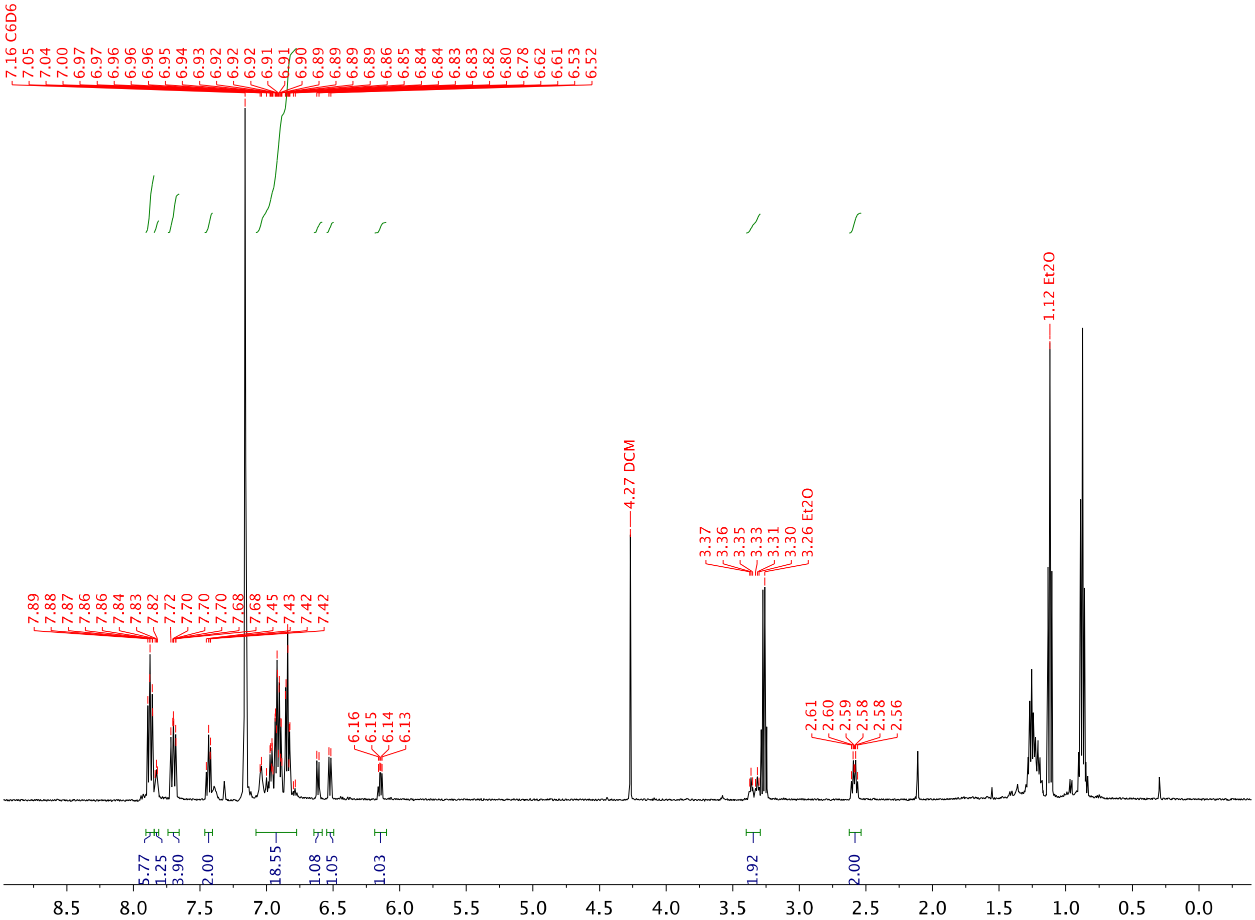

Figure S5. ^1H **NMR spectrum (500 MHz,** C_6D_6**) of 2.**

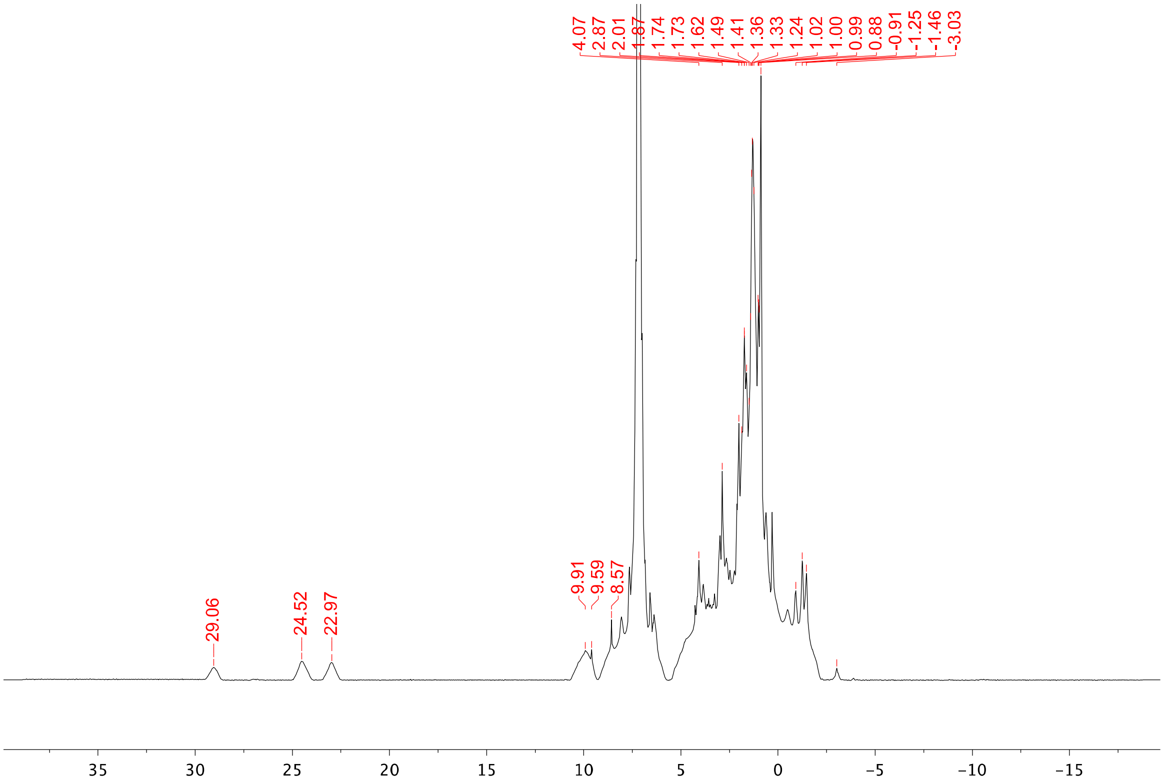

Figure S6. ^{1}H NMR spectrum (500 MHz, C_6D_6) of 3.

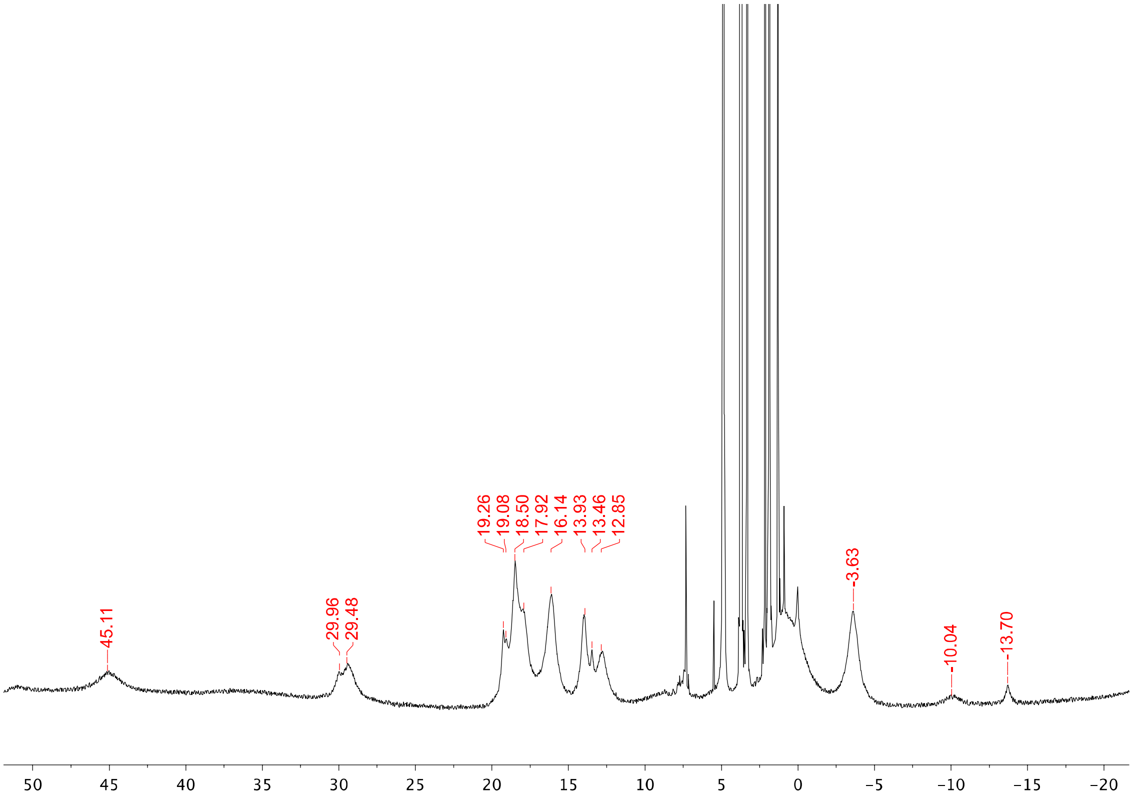

Figure S7. ^{1}H NMR spectrum (500 MHz, CD_3OD) of 4.

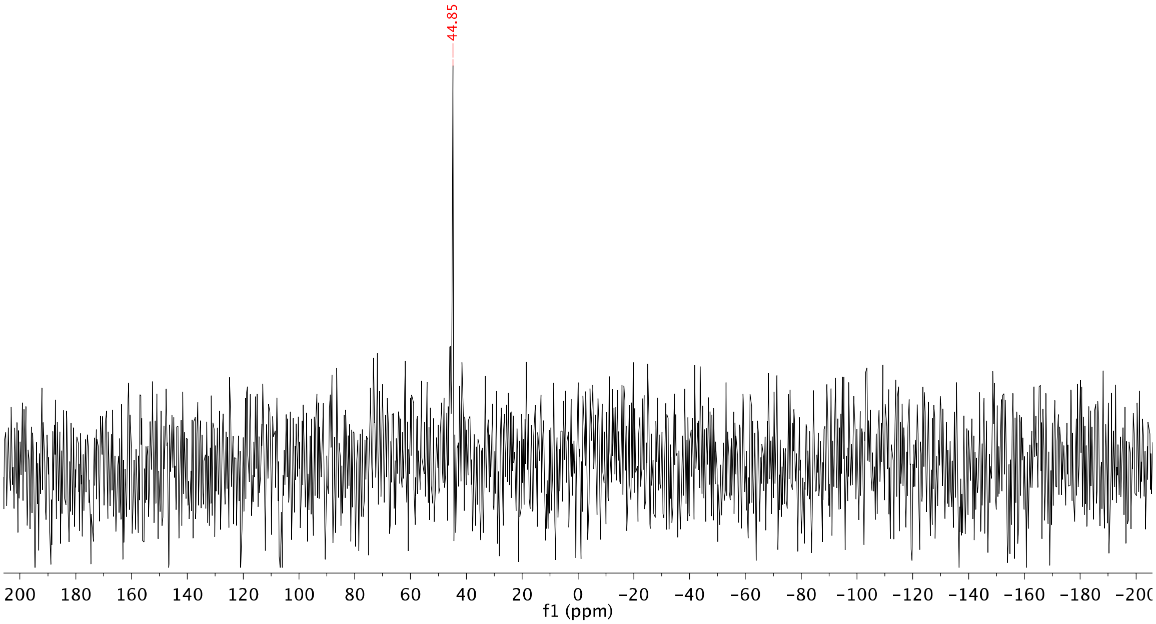

Figure S8. $^{31}P\{^{1}H\}$ NMR spectrum (202 MHz, $CDCl_3$) of 5(BF_4).

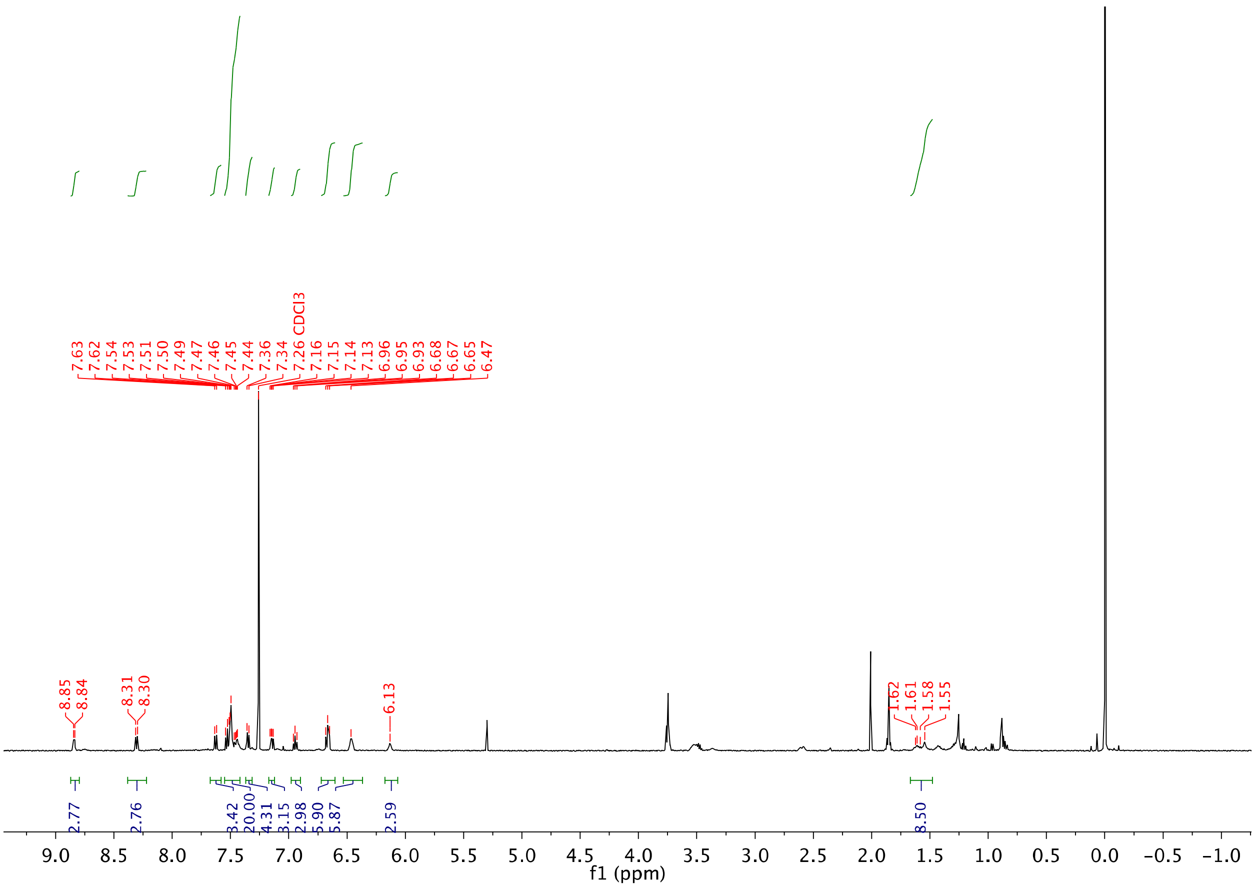

Figure S9. ^{1}H NMR spectrum (500 MHz, $CDCl_3$) of 5(BF_4).

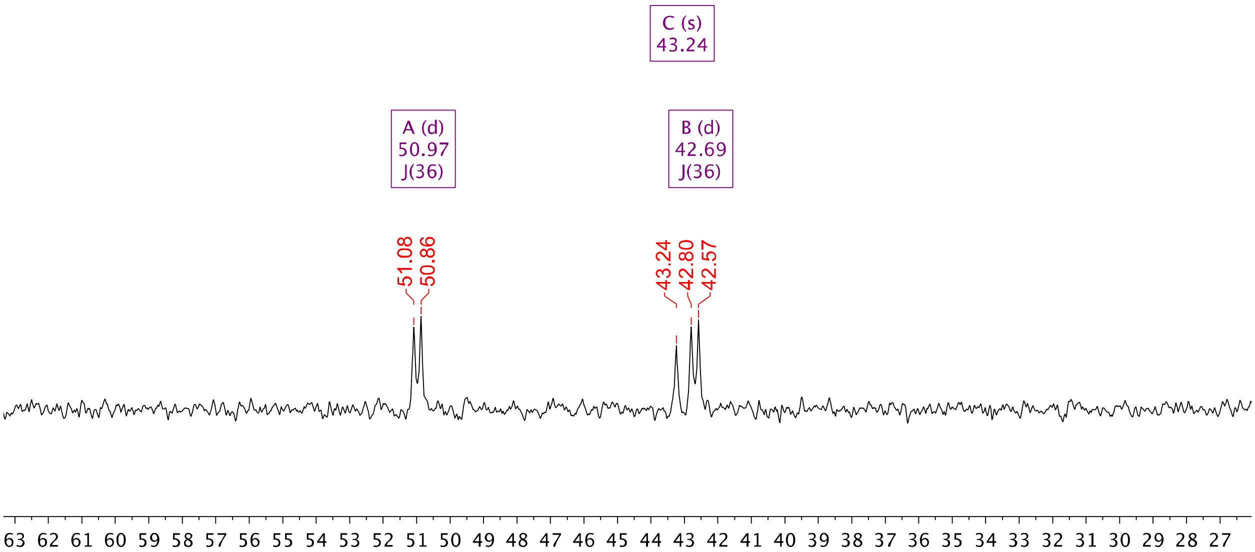

Figure S10. $^{31}P\{^1H\}$ NMR spectrum (202 MHz, CD_2Cl_2) of 5(BAr^F_4).

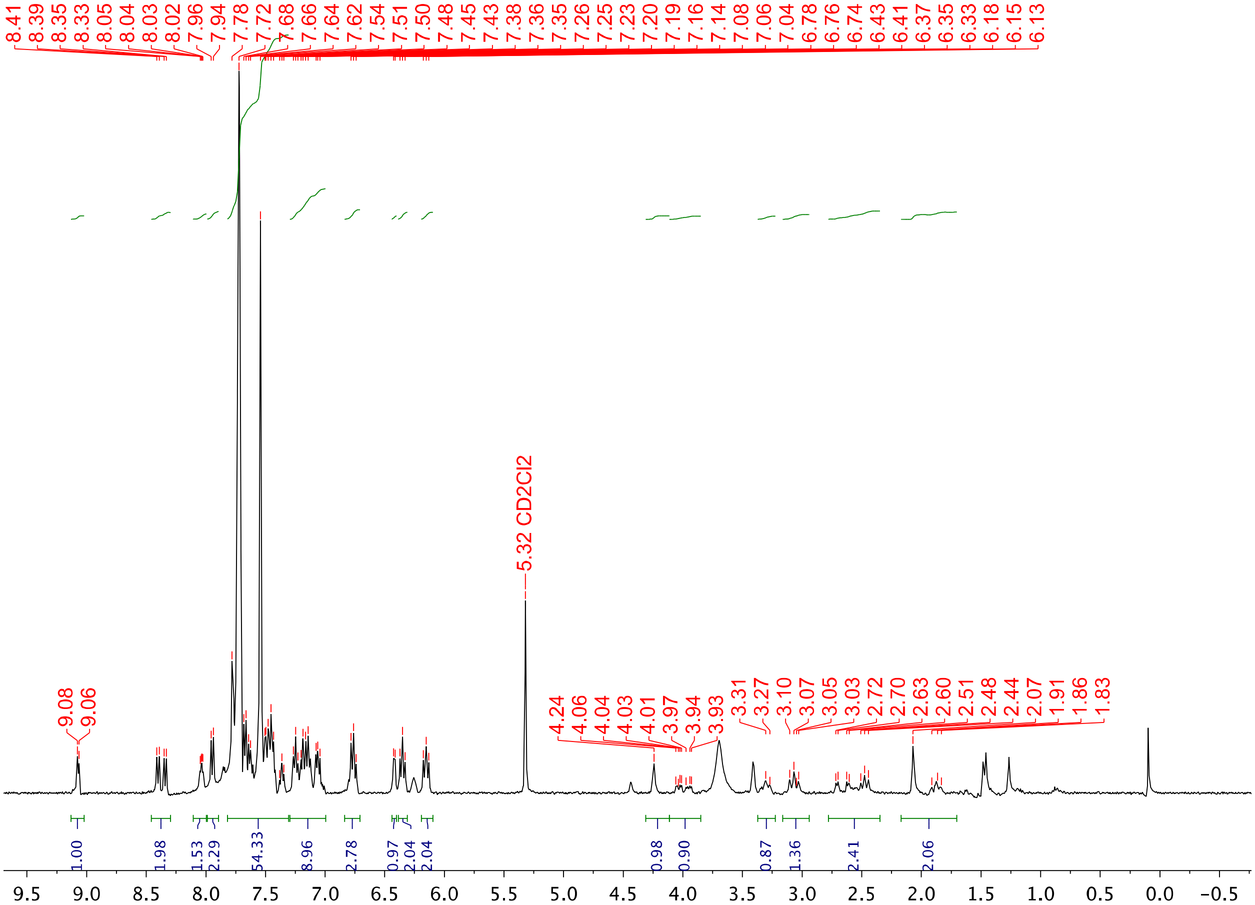

Figure S11. ^1H NMR spectrum (500 MHz, CD_2Cl_2) of 5(BAr^F_4).

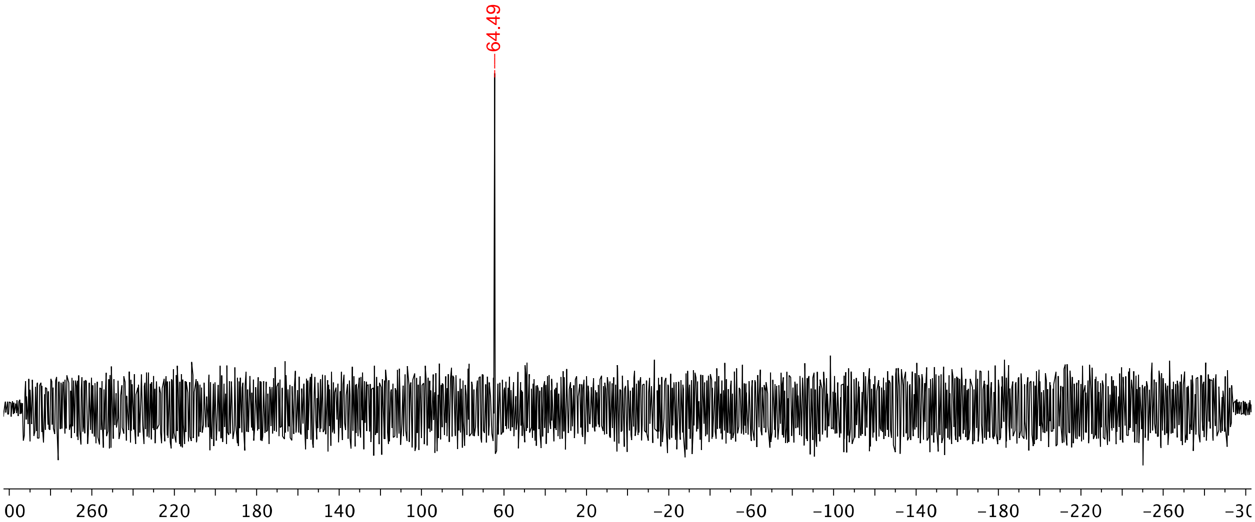

Figure Error! No text of specified style in document.**12. $^{31}P\{^1H\}$ NMR spectrum (242 MHz, C_6D_6) of 6.**

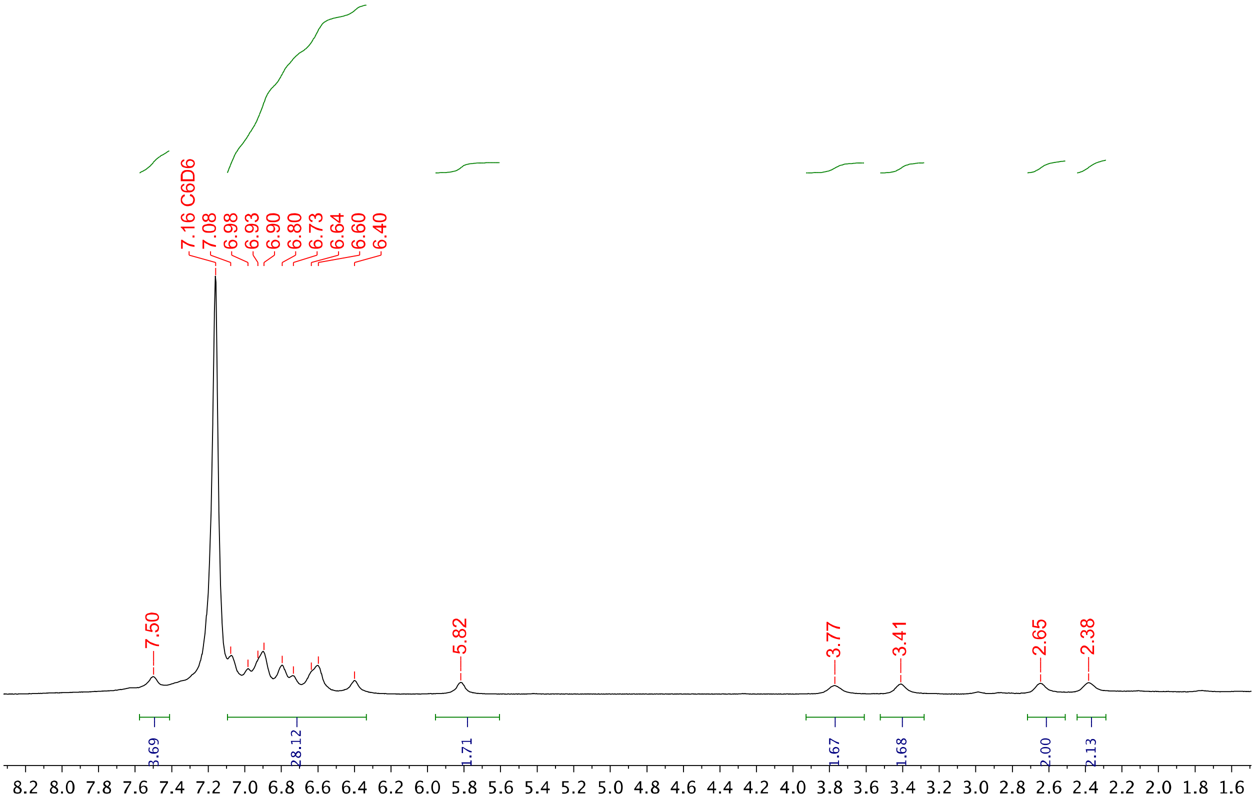

Figure Error! No text of specified style in document.**13. ^1H NMR spectrum (600 MHz, C_6D_6) of 6.**

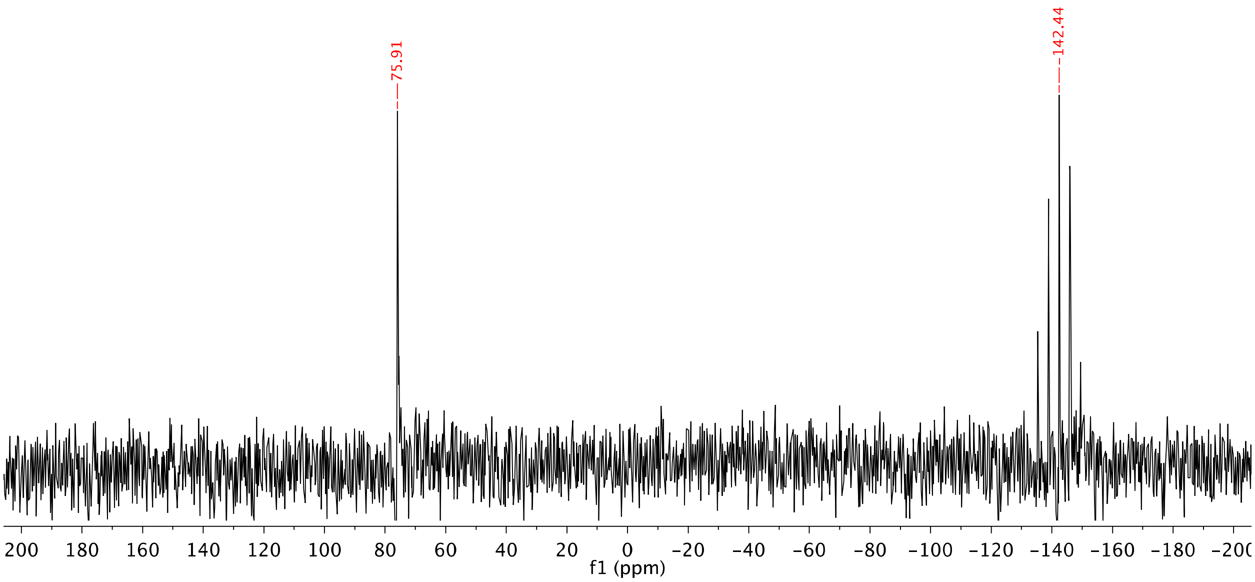

Figure Error! No text of specified style in document.**14. ^{31}P{^{1}H} NMR spectrum (202 MHz, C_6D_6) of 7.**

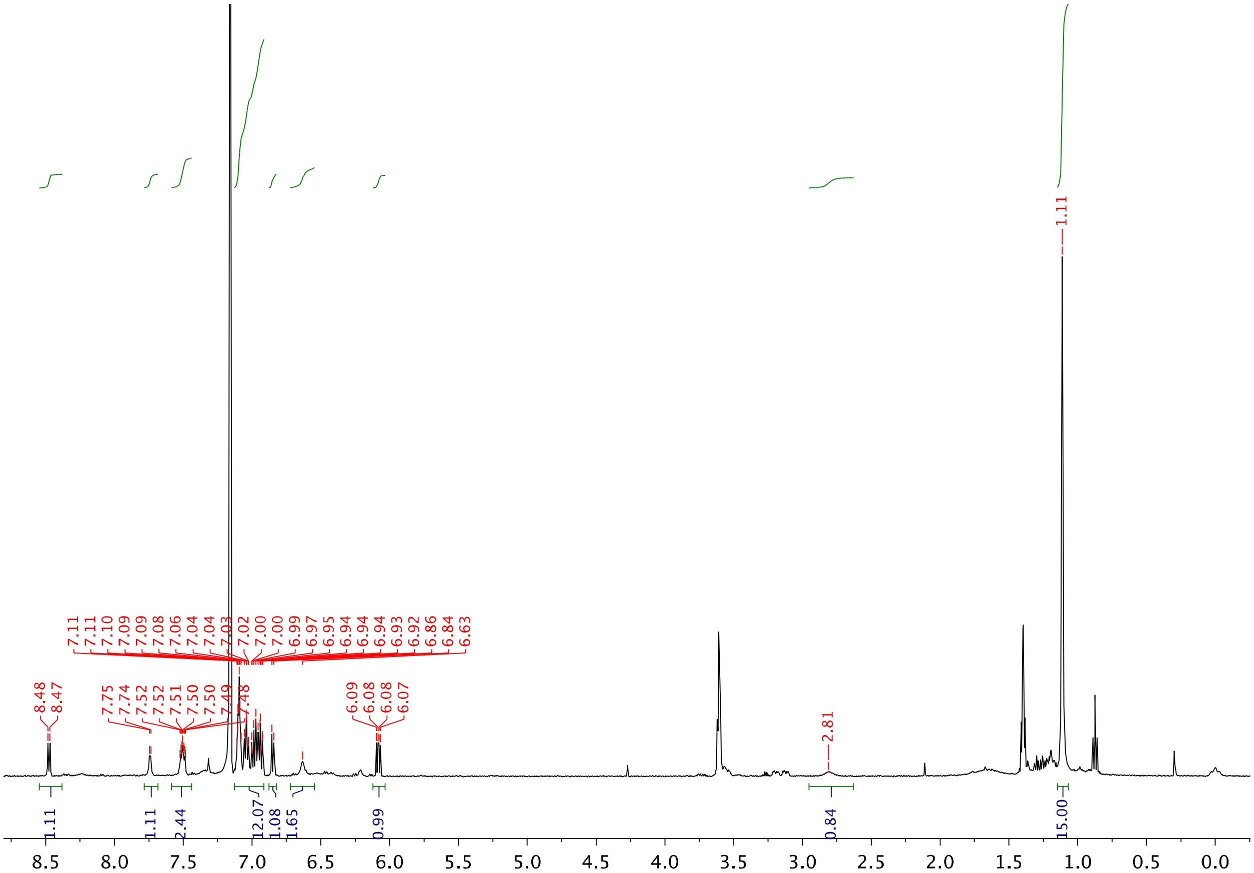

Figure Error! No text of specified style in document.**15. ^{1}H NMR spectrum (500 MHz, C_6D_6) of 7**

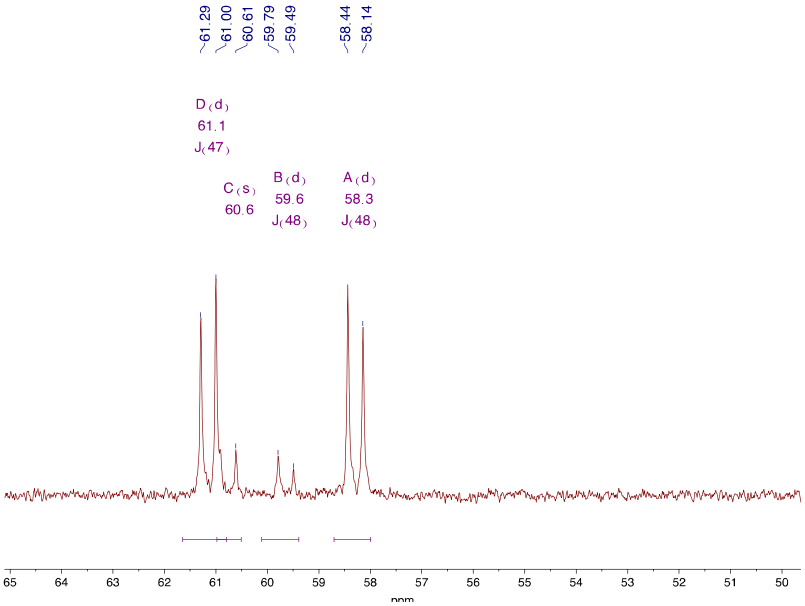

Figure S16. $^{31}P\{^1H\}$ NMR spectrum (202 MHz, THF, D_2O insert) of 5b(BAr^F_4).

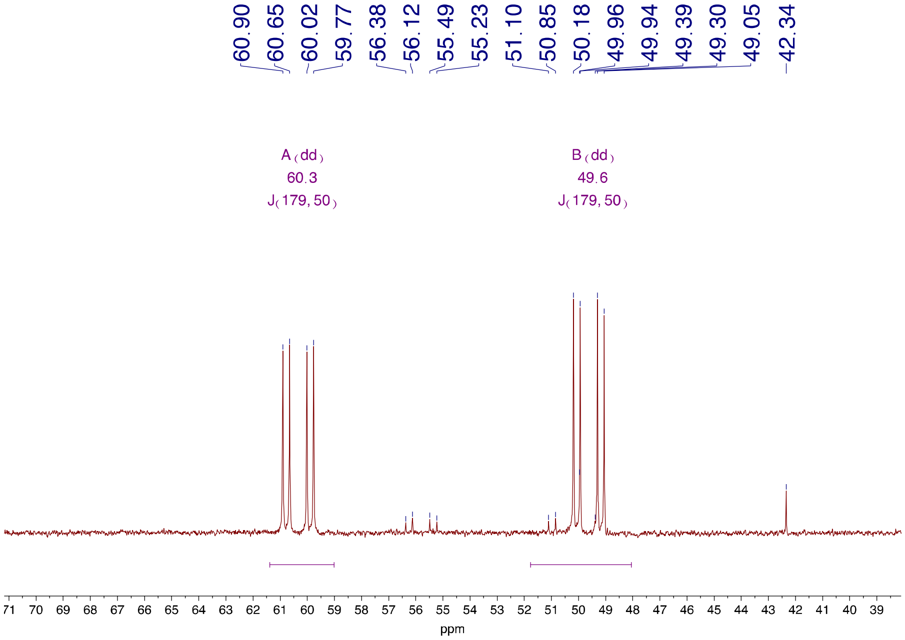

Figure S17. $^{31}P\{^1H\}$ NMR spectrum (202 MHz, THF, D_2O insert) of 2(BAr^F_4).

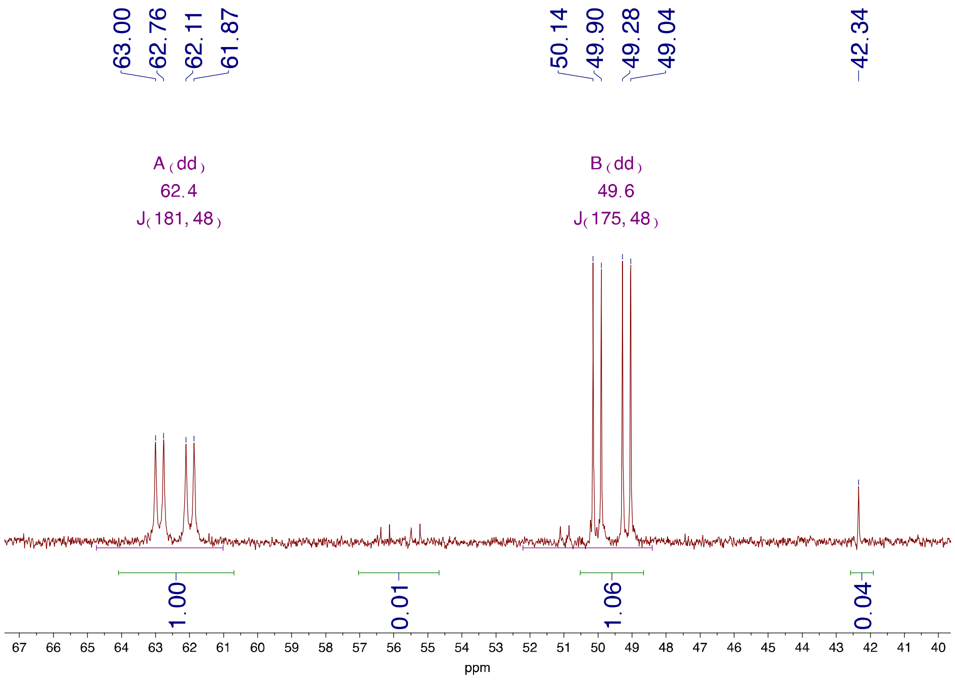

Figure S18. $^{31}P\{gated\ ^{1}H\}$ NMR spectrum (202 MHz, THF, D_2O insert) of the p*K*$_a$ study with complex 2($BAr^F{}_4$) and 1 equivalent of NEt_3.

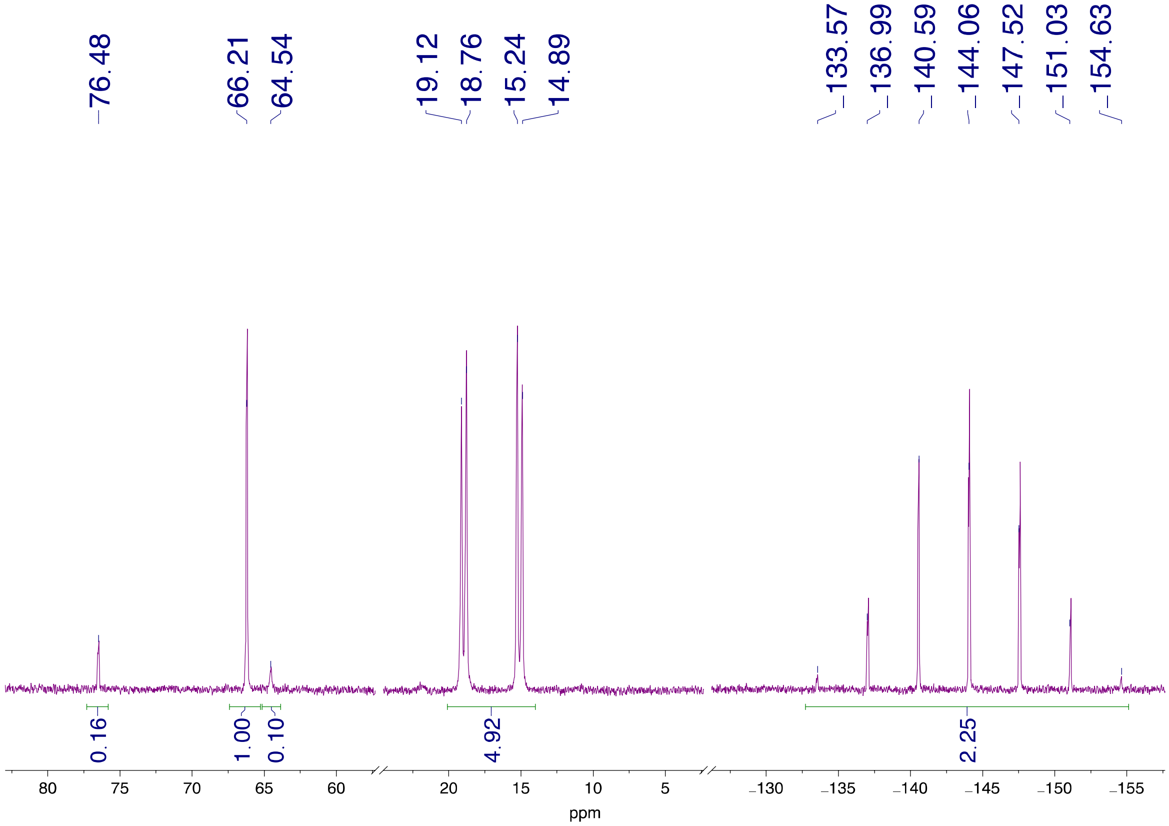

Figure S19. $^{31}P\{gated\ ^{1}H\}$ NMR spectrum (202 MHz, THF, D_2O insert) of the p*K*$_a$ study with complex 7 and 1 equivalent of phosphazene base P_2-Et.

$$K = \frac{[\text{Fe-NH-N}] \times [\text{Lut.-H}^{+}]}{[\text{Fe-NH-NH}] \times [\text{Lut.}]}$$

$$= \left(\frac{1.00 * 2 + 0.15 * 2}{0.32 * 2 + 0.31}\right)^{2}$$

since $[\text{Fe-NH-N}] = [\text{Lut.-H}^{+}]$
and $[\text{Fe-NH-NH}] = [\text{Lut.}]$

$$= \frac{k_a[Fe]}{k_a[lut.]}$$ $\mathrm{p}K_{\mathrm{a}}$ of Lut-H^{+} = 7.2

$\underline{\mathrm{p}K_{\mathrm{a}} = 6.4}$

Scheme S2. Calculation of 5(BAr$^{\mathrm{F}}{}_{4}$) pK_{a} from the ^{31}P{^{1}H} NMR in Figure 7a. Note the pK_{a} is an average of the two isomers as seen in Figure 7.

$$\text{Fraction deprotonated} = \frac{62.44 - 60.34}{67.30 - 60.34}$$

$$= 0.30$$

$$K = \frac{[\text{Rh-N}] \times [\text{TEA-H}^{+}]}{[\text{Rh-NH}] \times [\text{TEA}]}$$

$$= \left(\frac{0.30}{(1 - 0.30)}\right)^{2}$$

since $[\text{Rh-N}] = [\text{TEA-H}^{+}]$
and $[\text{Rh-NH}] = [\text{TEA}]$

$$= \frac{k_a[Rh - NH]}{k_a[\text{TEA}]}$$ $\mathrm{p}K_{\mathrm{a}}$ of TEA-H^{+} = 13.4

$\underline{\mathrm{p}K_{\mathrm{a}} = 14.1}$

Scheme S3. Calculation of 1(BAr$^{\mathrm{F}}{}_{4}$) pK_{a} from the ^{31}P{^{1}H} NMR in Figure 7b.

For the reaction: $\mathbf{5(BAr^F{}_4)}$ + lutidine $\overset{\text{K}}{\rightleftharpoons}$ $\mathbf{5b(BAr^F{}_4)}$ + lutidinium
the free energy change was calculated to be 8.3 kcal/mol.

K = 10 ^(-ΔG/RT)
= 10 ^(-1.5/(-0.0198*298))
= 0.08168

$$\text{K} = \frac{\text{[[5b(BAr}^{\text{F}}{}_4\text{][lutidinium]}}{\text{[5(BAr}^{\text{F}}{}_4\text{)][lutidine]}}$$

$$= \frac{\text{k}_\text{a}\text{(5(BAr}^{\text{F}}{}_4\text{))}}{\text{K}_\text{a}\text{(lutidine)}}$$

So k_a(5(BAr$^\text{F}{}_4$)) = K * k_a(lutidine)
= 0.08168 * 10^(-7.2)
= 5.15 * 10 ^ (-09)
So pk_a(5(BAr$^\text{F}{}_4$)) = 8.3

Scheme S4. DFT calculation example to calculate pK_a of 5(BAr$^F{}_4$). The experimental pK_a value for lutidine of 7.2 was used.[2]

$$K = \frac{\text{[Fe-N] x [Base-H}^+\text{]}}{\text{[Fe-NH] x [Base]}}$$

$$= \left(\frac{1.00}{0.16}\right)^2$$

since [Fe-N] = [Base-H$^+$]
and [Fe-NH] = [Base]

$$= \frac{k_a[FeNH]}{k_a[\text{Base}]} \qquad \text{p}K_\text{a} \text{ of Base-H}^+ = 25.3$$

$\underline{\text{p}K_\text{a} = 24}$

Scheme S5. Calculation of 7 pK_a from the ^{31}P{^{1}H} NMR in Figure 8. Base = phosphazene base P$_2$-Et.

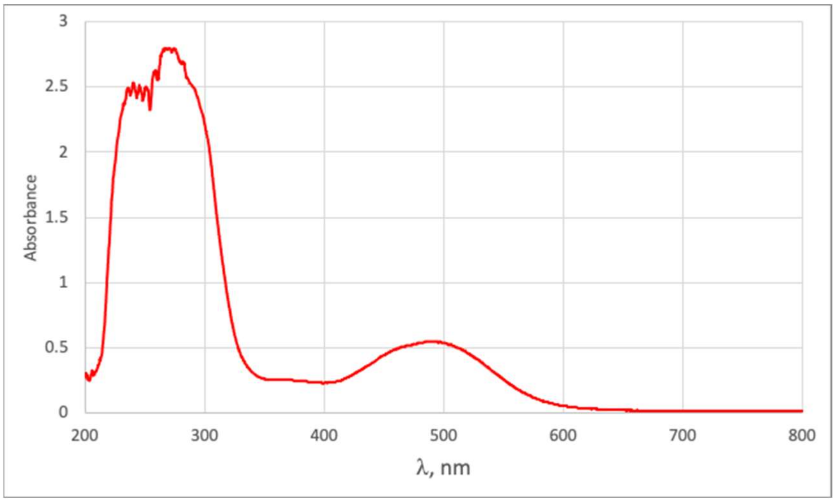

Figure S20. UV-Visible spectrum of $5(BAr^{F}_{4})$ in THF-red to orange solution.

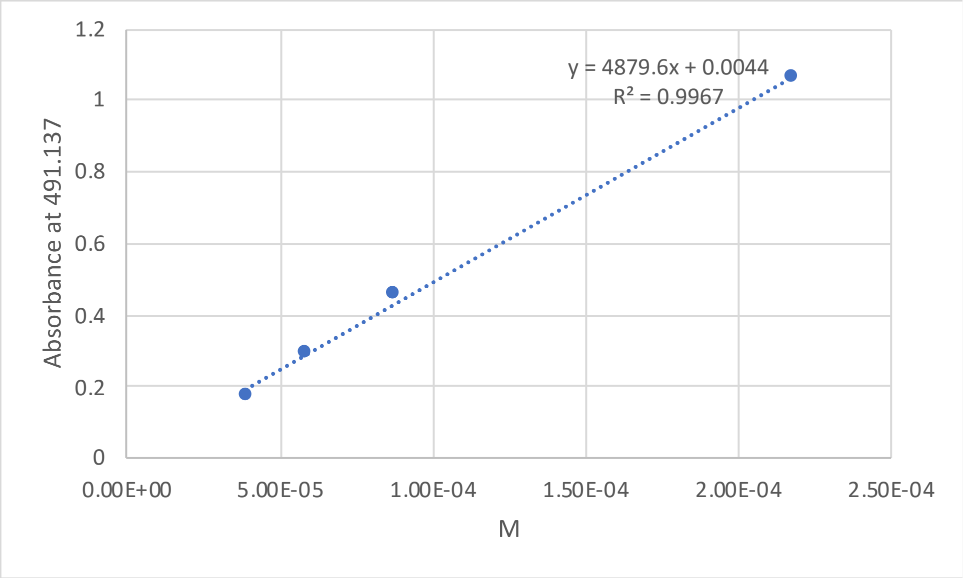

Figure S21. Beer-Lambert plot for UV-Visible spectrum of $5(BAr^{F}_{4})$. Spectra were taken in THF, with the peak centred at 491.137 nm used for the analysis.

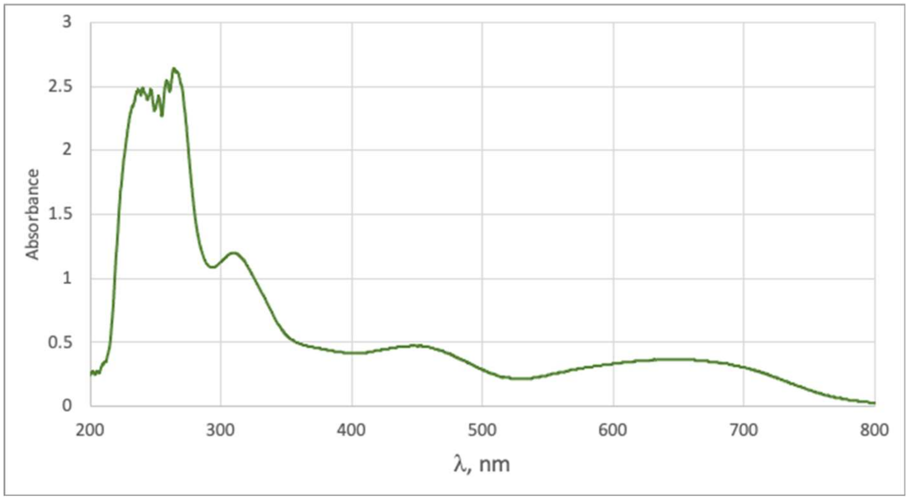

Figure S22. UV-Visible spectrum of 6 in THF- dark green solution.

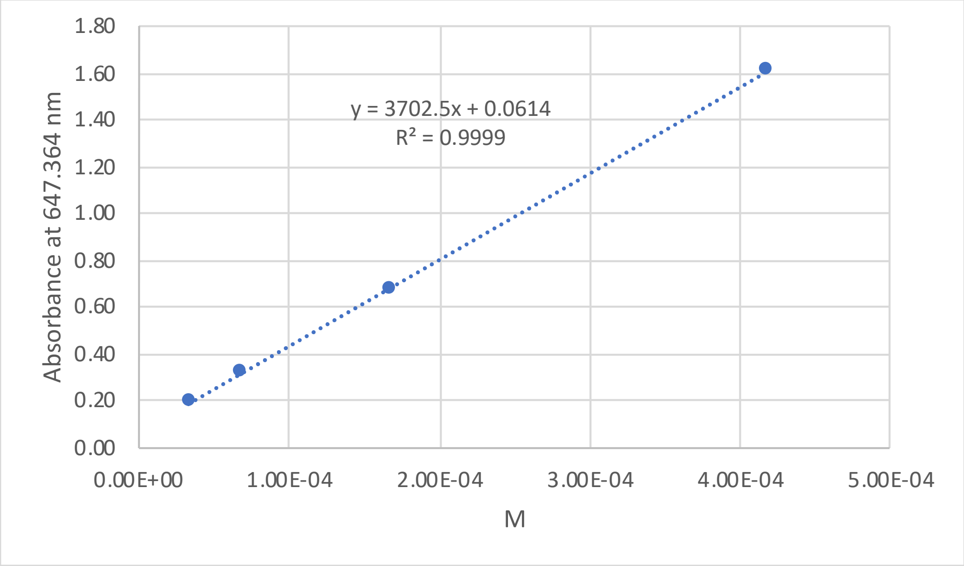

Figure S23. Beer-Lambert plot for UV-Visible spectrum of 6 in THF. Spectra were taken in THF, with the peak centred at 647.364 nm used for the analysis.

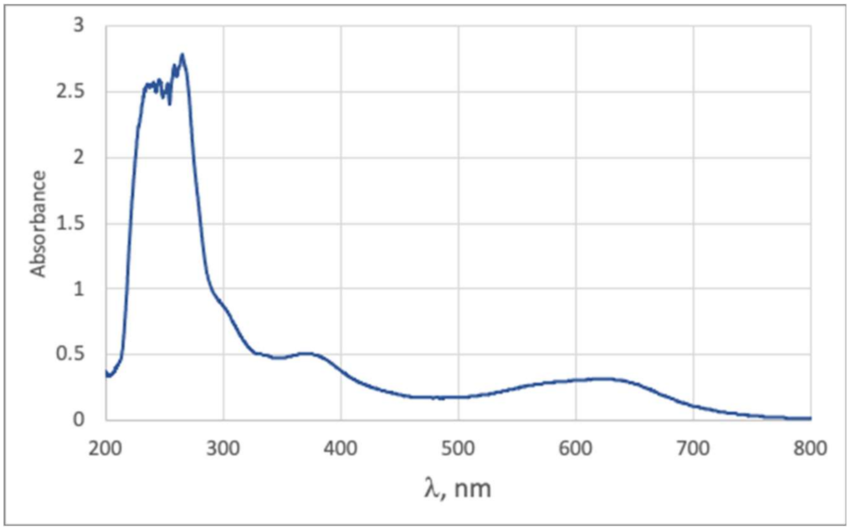

Figure S24. UV-Visible spectrum of 5b(BAr^F$_4$) in THF-dark blue solution.

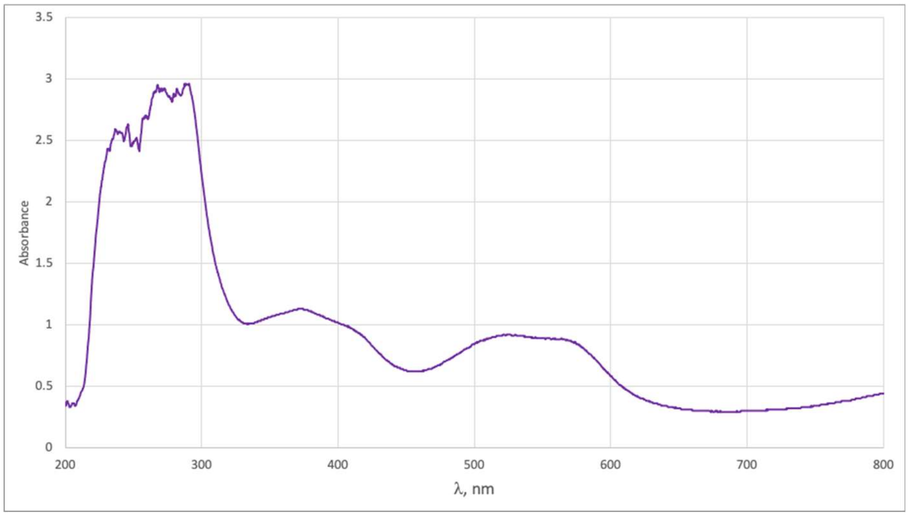

Figure S25. UV-Visible spectrum of the proposed Fe^{III} mono-protonated complex [Fe(L1^H)(L1)][(BAr^F$_4$)$_2$] in THF-dark purple/violet solution, from the reaction between TEMPO and 5(BAr^F$_4$).

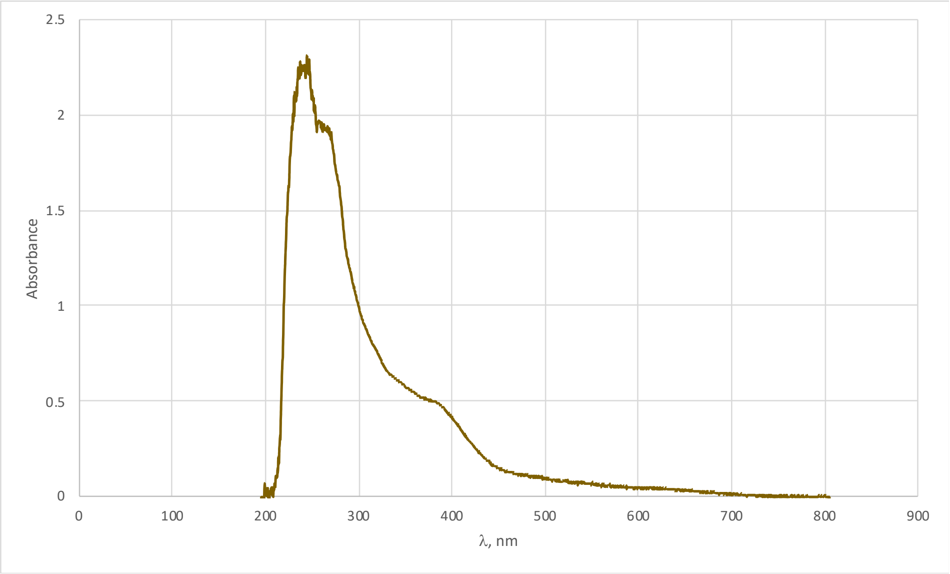

Figure S26. UV-Visible spectrum of 1(BAr^F$_4$) in THF-brown solution.

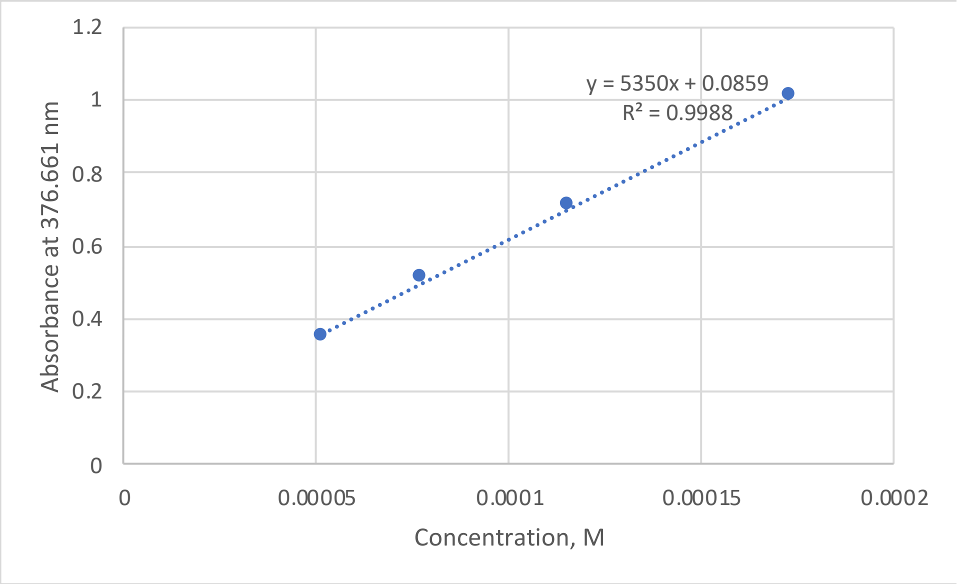

Figure S27. Beer-Lambert plot for UV-Visible spectrum of 1(BAr^F$_4$). Spectra were taken in THF, with the peak centred at 376.661 nm used for the analysis.

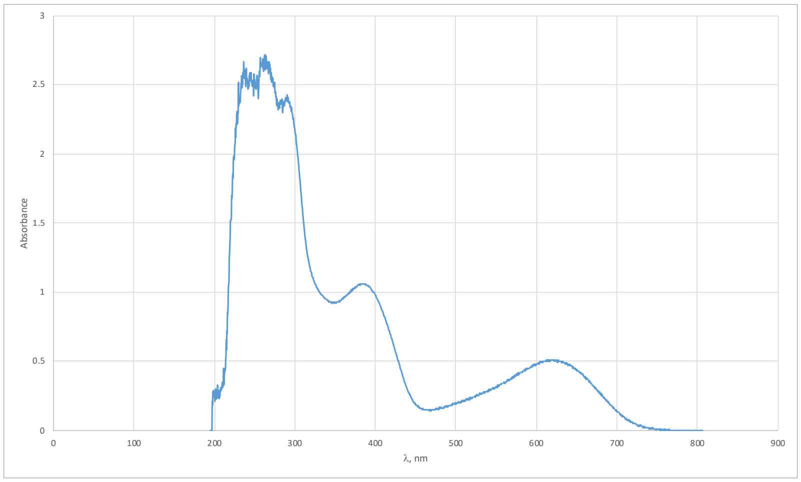

Figure S28. UV-Visible spectrum of 2 in THF-blue solution.

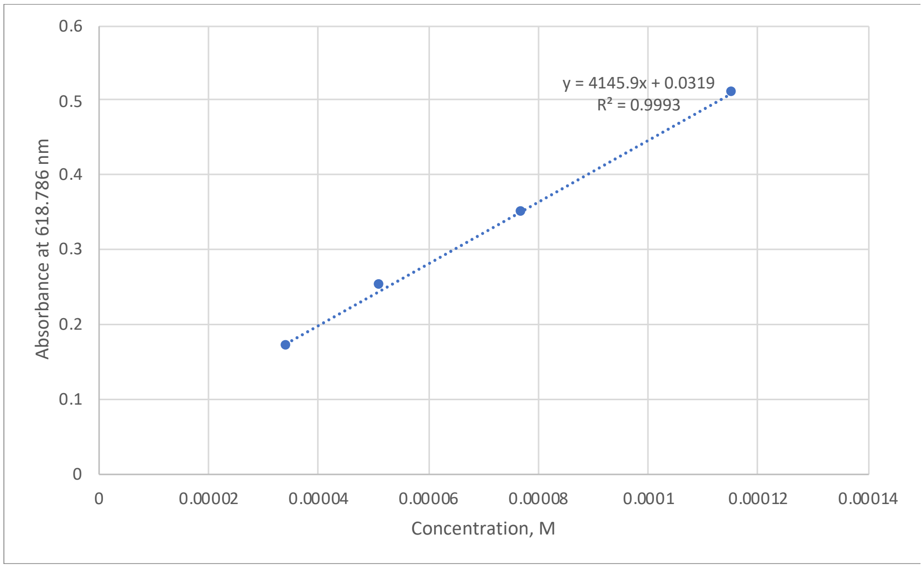

Figure S29. Beer-Lambert plot for UV-Visible spectrum of 2. Spectra were taken in THF, with the peak centred at 618.786 nm used for the analysis.

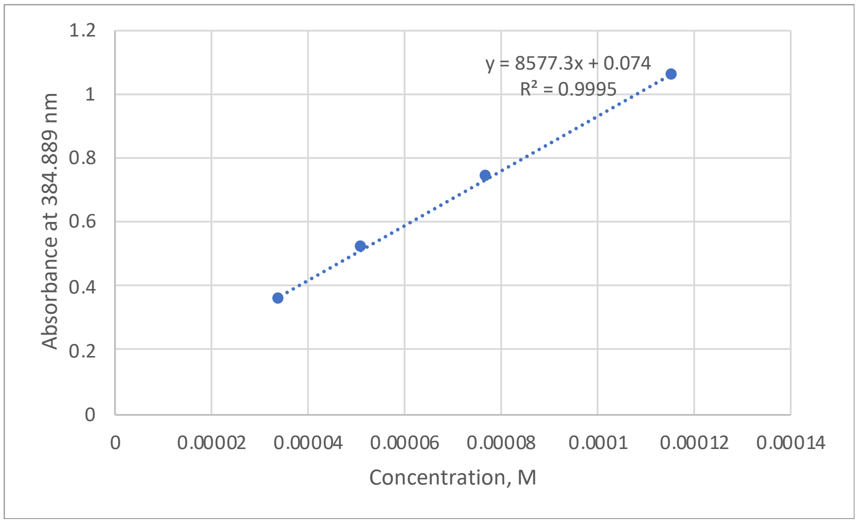

Figure S30. Beer-Lambert plot for UV-Visible spectrum of 2. Spectra were taken in THF, with the peak centred at 384.889 nm used for the analysis.

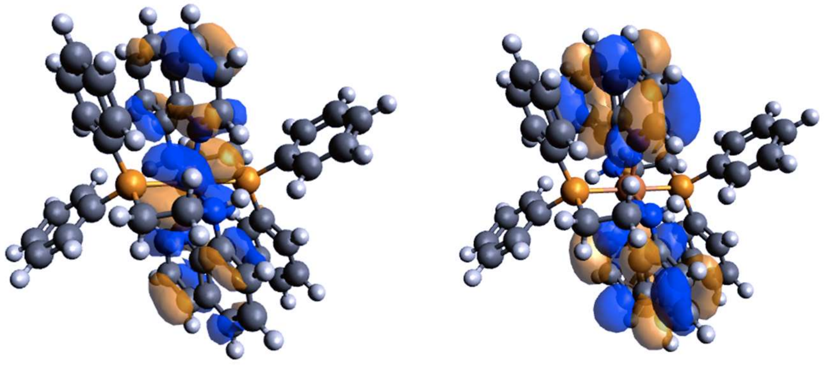

(a) HOMO LUMO

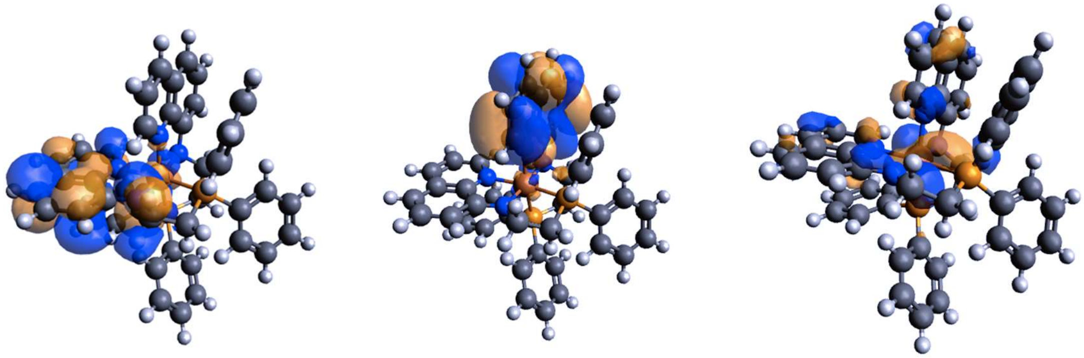

(b) HOMO LUMO HOMO -1

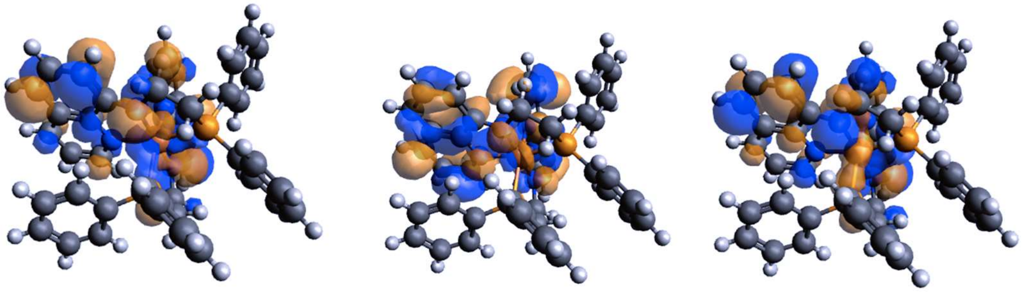

(c) HOMO LUMO HOMO-1

Figure S31. DFT calculated molecular orbitals of: (a) HOMO/LUMO for 5(BAr^{F}$_4$). The molecular orientation is the same as the chemdraw in Scheme 5. (b) HOMO/LUMO for 5b(BAr^{F}$_4$). (c) HOMO/LUMO/HOMO-1 for 6. Note the molecular orientations in (b) and (c) are approximately the same as the chemdraw Scheme 7 for complex 6.

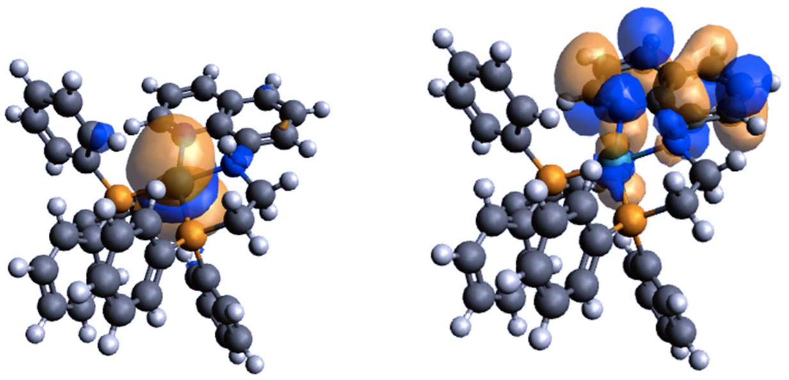

(a) HOMO LUMO

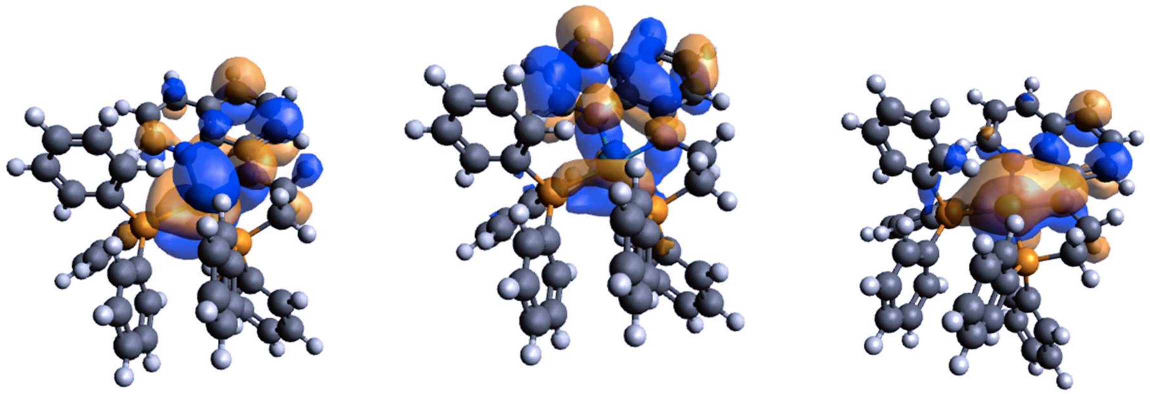

(b) HOMO LUMO HOMO-1

Figure S32. (a) HOMO/LUMO for 1(BAr$^{F}{}_{4}$). Note the molecular orientation is the approximately the same as the chemdraw in Scheme 1, except it is tilted on the z-axis for clarity. (b) HOMO/LUMO/HOMO-1 for 2. Note the molecular orientation is approximately the same as the chemdraw Scheme 2, except it is tilted on the z-axis for clarity.

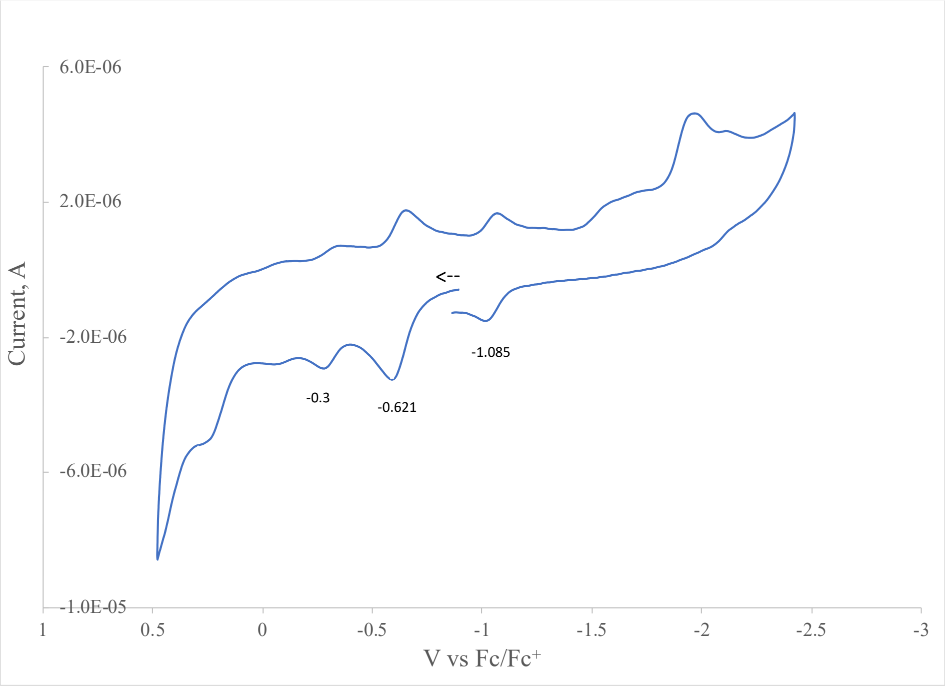

Figure S33. Cyclic voltammogram of 5b(BAr$^F{}_4$).

BDFE = 1.37[pK_a] + 23.06[$E_{1/2}$] + C_G

= 1.37[6.4] + 23.06[-0.621] + 60.4

BDFE of N-H = 54.9 kcal/mol

Scheme S6. Calculation of N–H BDFE for 5(BAr$^F{}_4$). C_G is a constant that varies with solvent; the value for THF used here is from reference 3.[3]

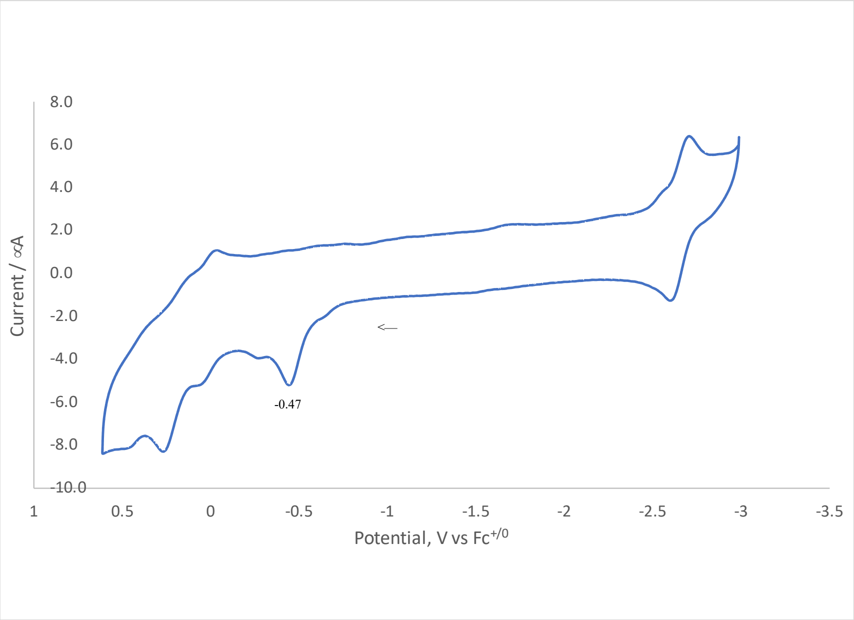

(a)

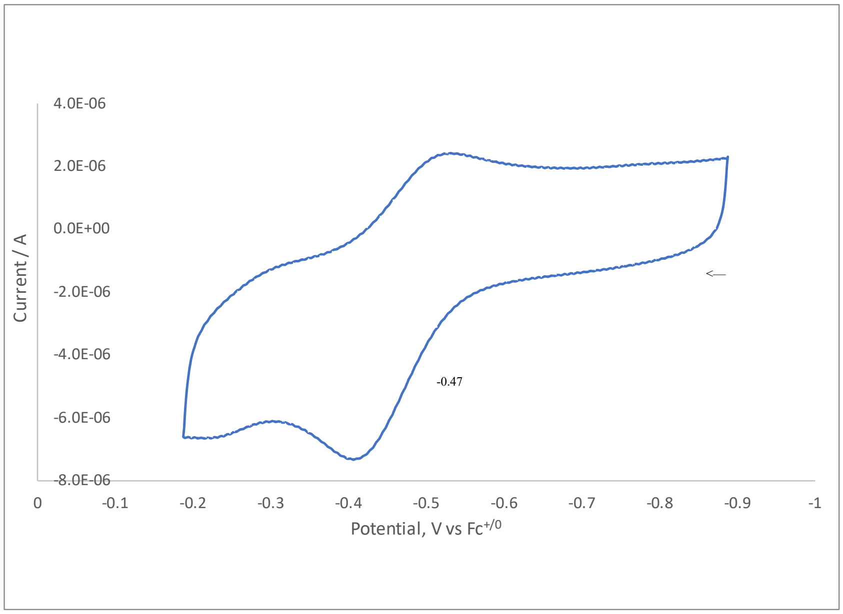

(b)

Figure S34. Cyclic voltammogram of 2. (a) Wide scan window at 100 mV/second. (b) Narrow scan window at 500 mV/second.

$$\begin{aligned}\text{BDFE} &= 1.37[\text{p}K_a] + 23.06[E_{1/2}] + C_G \\ &= 1.37[14.1] + 23.06[-0.47] + 60.4\end{aligned}$$

BDFE of N-H = 69 kcal/mol

Scheme S7. Calculation of N–H BDFE for 1(BAr^F$_4$). C$_G$ is a constant that varies with solvent; the value for THF used here is from reference 2.

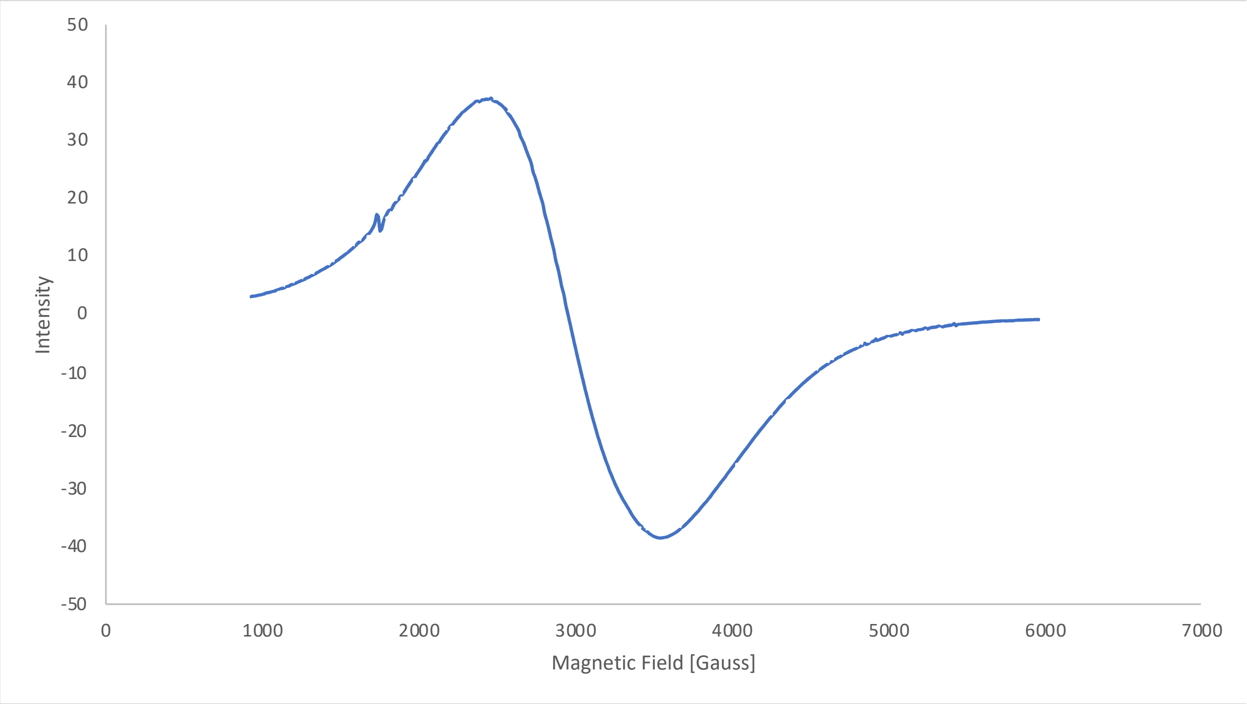

Figure S35. Solution electron paramagnetic resonance (EPR) spectrum of proposed Fe^{III} complex [Fe(L1^H)(L1)][(Bar^F$_4$)$_2$] from the reaction between 5(BAr^F$_4$) and TEMPO. The g-value is 2.36. Taken in diethyl ether in a J-young tube, at room temperature. The microwave frequency was 9751.66 MHz. The sample was referenced to DPPH.

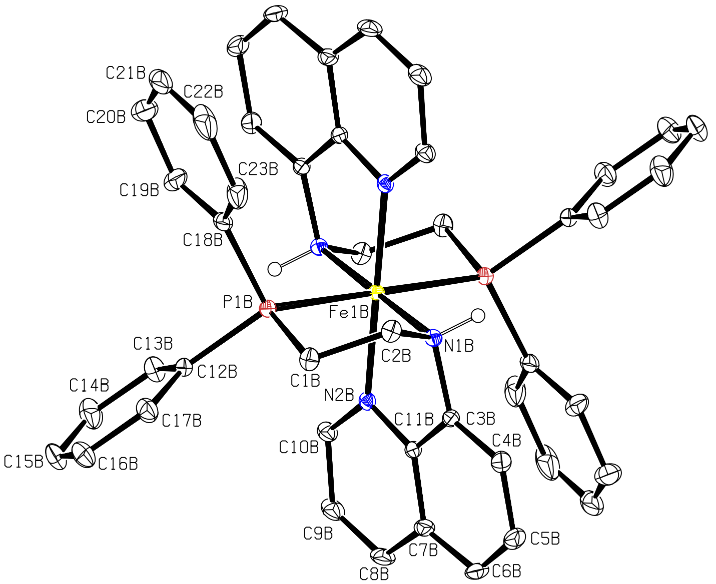

Figure S36. X-ray diffraction-derived structure of 5(BF_4). Ellipsoids are shown at 30% probability. Carbon-bound hydrogen atoms and anions have been omitted for clarity. There were two independent molecules in the asymmetric unit for 5(BF_4). Molecule B is shown here, and molecule A is provided in the manuscript Figure 4.

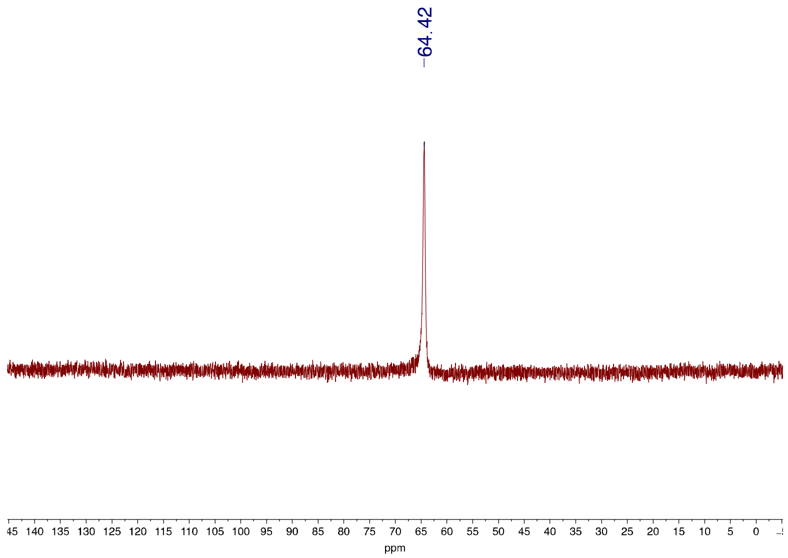

Figure S37. $^{31}P\{^1H\}$ **NMR spectrum (202 MHz,** C_6D_6**) of the attempted synthesis of the amido complex of 7.**

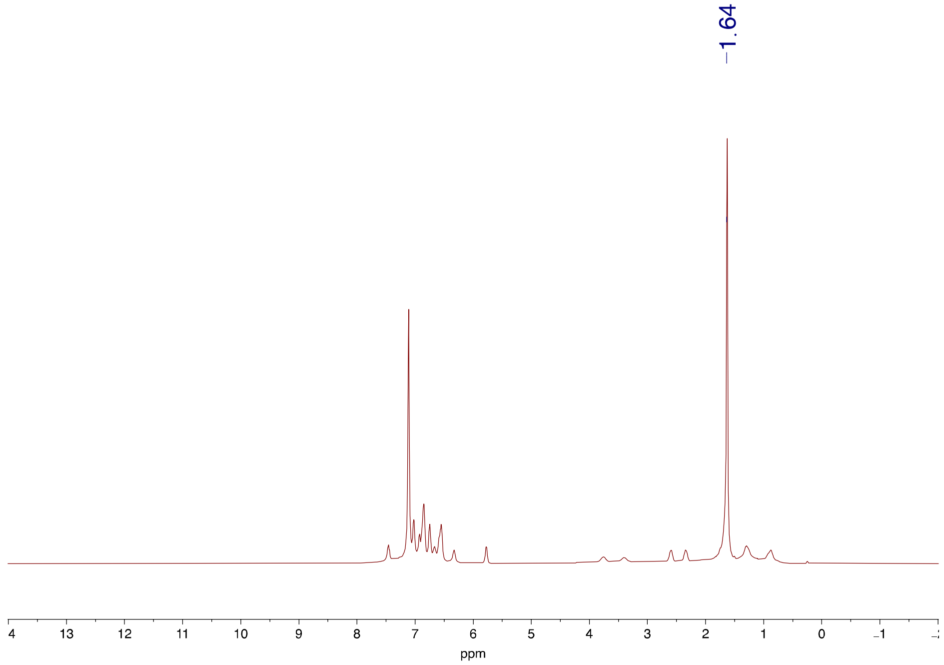

Figure S38. ^1H **NMR spectrum (500 MHz,** C_6D_6**) of the attempted synthesis of the amido complex of 7.**

Table S1. Crystal data and structure refinement for 1.

Identification code	d18135_a	
Empirical formula	C42 H38 Cl3 N2 P2 Rh	
Formula weight	841.94	
Temperature	150(2) K	
Wavelength	0.71073 Å	
Crystal system	Monoclinic	
Space group	P2_1/c	
Unit cell dimensions	a = 11.0823(12) Å	a= 90°.
	b = 19.724(2) Å	b= 97.340(3)°.
	c = 17.977(2) Å	g = 90°.
Volume	3897.4(8) Å^3	
Z	4	
Density (calculated)	1.435 Mg/m^3	
Absorption coefficient	0.758 mm^{-1}	
F(000)	1720	
Crystal size	0.250 x 0.120 x 0.120 mm^3	
Theta range for data collection	1.540 to 27.555°.	
Index ranges	-14<=h<=14, -25<=k<=25, -23<=l<=23	
Reflections collected	78494	
Independent reflections	8994 [R(int) = 0.1007]	
Completeness to theta = 25.242°	100.0 %	
Absorption correction	Semi-empirical from equivalents	
Max. and min. transmission	0.7456 and 0.6948	
Refinement method	Full-matrix least-squares on F^2	
Data / restraints / parameters	8994 / 57 / 483	
Goodness-of-fit on F^2	0.997	
Final R indices [I>2sigma(I)]	R1 = 0.0372, wR2 = 0.0647	
R indices (all data)	R1 = 0.0838, wR2 = 0.0778	
Extinction coefficient	n/a	
Largest diff. peak and hole	0.714 and -0.916 e.Å^{-3}	

Table S2. Crystal data and structure refinement for 2.

Identification code	d2119_a	
Empirical formula	C41 H35 N2 P2 Rh	
Formula weight	720.56	
Temperature	150(2) K	
Wavelength	1.54178 Å	
Crystal system	Orthorhombic	
Space group	Pbca	
Unit cell dimensions	a = 16.7058(8) Å	a= 90°.
	b = 17.8410(9) Å	b= 90°.
	c = 21.8589(12) Å	g = 90°.
Volume	6515.0(6) Å^3	
Z	8	
Density (calculated)	1.469 Mg/m^3	
Absorption coefficient	5.417 mm^{-1}	
F(000)	2960	
Crystal size	0.450 x 0.030 x 0.030 mm^3	
Theta range for data collection	4.151 to 65.893°.	
Index ranges	-19<=h<=19, -21<=k<=21, -25<=l<=25	
Reflections collected	114227	
Independent reflections	5623 [R(int) = 0.1464]	
Completeness to theta = 65.893°	99.2 %	
Absorption correction	Semi-empirical from equivalents	
Max. and min. transmission	0.7527 and 0.5072	
Refinement method	Full-matrix least-squares on F^2	
Data / restraints / parameters	5623 / 0 / 416	
Goodness-of-fit on F^2	1.038	
Final R indices [I>2sigma(I)]	R1 = 0.0404, wR2 = 0.0920	
R indices (all data)	R1 = 0.0551, wR2 = 0.0999	
Extinction coefficient	0.00076(5)	
Largest diff. peak and hole	0.734 and -0.902 e.Å^{-3}	

Table S1. Crystal data and structure refinement for 3.

Identification code	d18150_a	
Empirical formula	C23 H32 Cl Co N2 P	
Formula weight	461.85	
Temperature	150(2) K	
Wavelength	1.54178 Å	
Crystal system	Monoclinic	
Space group	$P2_1$	
Unit cell dimensions	a = 6.9916(9) Å	a= 90°.
	b = 9.4534(10) Å	b= 98.836(9)°.
	c = 16.8751(19) Å	g = 90°.
Volume	1102.1(2) Å^3	
Z	2	
Density (calculated)	1.392 Mg/m^3	
Absorption coefficient	7.976 mm^{-1}	
F(000)	486	
Crystal size	0.150 x 0.030 x 0.010 mm^3	
Theta range for data collection	2.650 to 67.207°.	
Index ranges	-8<=h<=8, -11<=k<=11, -20<=l<=19	
Reflections collected	18447	
Independent reflections	3837 [R(int) = 0.1254]	
Completeness to theta = 67.207°	99.2 %	
Absorption correction	Semi-empirical from equivalents	
Max. and min. transmission	0.7529 and 0.4886	
Refinement method	Full-matrix least-squares on F^2	
Data / restraints / parameters	3837 / 1 / 254	
Goodness-of-fit on F^2	0.998	
Final R indices [I>2sigma(I)]	R1 = 0.0648, wR2 = 0.1636	
R indices (all data)	R1 = 0.0809, wR2 = 0.1757	
Absolute structure parameter	0.036(11)	
Extinction coefficient	n/a	
Largest diff. peak and hole	0.622 and -0.756 e.Å-3	

Table S4. Crystal data and structure refinement for 4.

Identification code	d1927_a	
Empirical formula	C50 H58 Cl4 N4 Ni2 O4 P2	
Formula weight	1100.16	
Temperature	150(2) K	
Wavelength	1.54178 Å	
Crystal system	Monoclinic	
Space group	$P2_1/n$	
Unit cell dimensions	a = 10.7663(3) Å	a= 90°.
	b = 16.4614(4) Å	b= 90.7850(10)°.
	c = 14.4611(3) Å	g = 90°.
Volume	2562.68(11) Å^3	
Z	2	
Density (calculated)	1.426 Mg/m^3	
Absorption coefficient	3.799 mm^{-1}	
F(000)	1144	
Crystal size	0.180 x 0.040 x 0.040 mm^3	
Theta range for data collection	4.069 to 68.710°.	
Index ranges	-12<=h<=11, -19<=k<=19, -17<=l<=17	
Reflections collected	41158	
Independent reflections	4599 [R(int) = 0.0933]	
Completeness to theta = 67.679°	99.0 %	
Absorption correction	Semi-empirical from equivalents	
Max. and min. transmission	0.7529 and 0.6194	
Refinement method	Full-matrix least-squares on F^2	
Data / restraints / parameters	4599 / 0 / 302	
Goodness-of-fit on F^2	1.053	
Final R indices [I>2sigma(I)]	R1 = 0.0326, wR2 = 0.0853	
R indices (all data)	R1 = 0.0519, wR2 = 0.0910	
Extinction coefficient	n/a	
Largest diff. peak and hole	0.532 and -0.671 e.Å^{-3}	

Table S2. Crystal data and structure refinement for 5(BF$_4$).

Identification code	d1911_a	
Empirical formula	C48 H46 B2 Cl4 F8 Fe N4 P2	
Formula weight	1112.10	
Temperature	150(2) K	
Wavelength	0.71073 Å	
Crystal system	Triclinic	
Space group	P-1	
Unit cell dimensions	a = 11.0025(4) Å	a= 85.179(1)°.
	b = 13.0919(5) Å	b= 86.803(1)°.
	c = 16.8984(5) Å	g = 85.563(2)°.
Volume	2415.25(15) Å^{3}	
Z	2	
Density (calculated)	1.529 Mg/m^{3}	
Absorption coefficient	0.671 mm^{-1}	
F(000)	1136	
Crystal size	0.240 x 0.100 x 0.070 mm^{3}	
Theta range for data collection	1.211 to 27.666°.	
Index ranges	-14<=h<=14, -17<=k<=17, -21<=l<=21	
Reflections collected	78530	
Independent reflections	11228 [R(int) = 0.0627]	
Completeness to theta = 25.242°	100.0 %	
Absorption correction	Semi-empirical from equivalents	
Max. and min. transmission	0.7456 and 0.7029	
Refinement method	Full-matrix least-squares on F^{2}	
Data / restraints / parameters	11228 / 0 / 652	
Goodness-of-fit on F^{2}	1.004	
Final R indices [I>2sigma(I)]	R1 = 0.0384, wR2 = 0.0787	
R indices (all data)	R1 = 0.0723, wR2 = 0.0923	
Extinction coefficient	n/a	
Largest diff. peak and hole	0.704 and -0.411 e.Å^{-3}	

Table S3. Crystal data and structure refinement for 5(BAr^F_4).

Identification code	d2079_a	
Empirical formula	C112 H70 B2 Cl4 F48 Fe N4 P2	
Formula weight	2664.93	
Temperature	150(2) K	
Wavelength	1.54178 Å	
Crystal system	Monoclinic	
Space group	$P2_1/c$	
Unit cell dimensions	a = 12.6141(4) Å	a= 90°.
	b = 18.3139(6) Å	b= 95.214(2)°.
	c = 24.3958(8) Å	g = 90°.
Volume	5612.4(3) $Å^3$	
Z	2	
Density (calculated)	1.577 Mg/m^3	
Absorption coefficient	3.404 mm^{-1}	
F(000)	2672	
Crystal size	0.300 x 0.150 x 0.060 mm^3	
Theta range for data collection	3.022 to 66.179°.	
Index ranges	-14<=h<=14, -21<=k<=21, -28<=l<=28	
Reflections collected	161070	
Independent reflections	9636 [R(int) = 0.0521]	
Completeness to theta = 66.179°	98.2 %	
Absorption correction	Semi-empirical from equivalents	
Max. and min. transmission	0.7527 and 0.5307	
Refinement method	Full-matrix least-squares on F^2	
Data / restraints / parameters	9636 / 72 / 850	
Goodness-of-fit on F^2	1.027	
Final R indices [I>2sigma(I)]	R1 = 0.0492, wR2 = 0.1224	
R indices (all data)	R1 = 0.0545, wR2 = 0.1265	
Extinction coefficient	n/a	
Largest diff. peak and hole	0.630 and -0.658 e.$Å^{-3}$	

Table S4. Crystal data and structure refinement for 6.

Identification code	d18191_a	
Empirical formula	C46 H40 Fe N4 P2	
Formula weight	766.61	
Temperature	150(2) K	
Wavelength	0.71073 Å	
Crystal system	Monoclinic	
Space group	$P2_1/c$	
Unit cell dimensions	a = 18.3954(9) Å	a= 90°.
	b = 10.9104(4) Å	b= 112.720(2)°.
	c = 19.8924(9) Å	g = 90°.
Volume	3682.6(3) $Å^3$	
Z	4	
Density (calculated)	1.383 Mg/m^3	
Absorption coefficient	0.537 mm^{-1}	
F(000)	1600	
Crystal size	0.160 x 0.100 x 0.060 mm^3	
Theta range for data collection	2.076 to 27.595°.	
Index ranges	-23<=h<=23, -14<=k<=14, -19<=l<=25	
Reflections collected	47540	
Independent reflections	8505 [R(int) = 0.1145]	
Completeness to theta = 25.242°	100.0 %	
Absorption correction	Semi-empirical from equivalents	
Max. and min. transmission	0.7456 and 0.6471	
Refinement method	Full-matrix least-squares on F^2	
Data / restraints / parameters	8505 / 0 / 478	
Goodness-of-fit on F^2	0.997	
Final R indices [I>2sigma(I)]	R1 = 0.0468, wR2 = 0.0865	
R indices (all data)	R1 = 0.1088, wR2 = 0.1025	
Extinction coefficient	n/a	
Largest diff. peak and hole	0.750 and -0.488 e.$Å^{-3}$	

Table S8. Crystal data and structure refinement for 7.

Identification code	d2070_a	
Empirical formula	C33 H36 F6 Fe N2 P2	
Formula weight	692.43	
Temperature	150(2) K	
Wavelength	0.71073 Å	
Crystal system	Orthorhombic	
Space group	$P2_12_12_1$	
Unit cell dimensions	a = 12.8865(5) Å	a= 90°.
	b = 13.4261(5) Å	b= 90°.
	c = 18.1572(7) Å	g = 90°.
Volume	3141.5(2) Å^3	
Z	4	
Density (calculated)	1.464 Mg/m^3	
Absorption coefficient	0.644 mm^{-1}	
F(000)	1432	
Crystal size	0.170 x 0.150 x 0.130 mm^3	
Theta range for data collection	1.886 to 28.322°.	
Index ranges	-16<=h<=17, -17<=k<=17, -23<=l<=21	
Reflections collected	71768	
Independent reflections	7665 [R(int) = 0.0942]	
Completeness to theta = 25.242°	99.9 %	
Absorption correction	Semi-empirical from equivalents	
Max. and min. transmission	0.7456 and 0.7009	
Refinement method	Full-matrix least-squares on F^2	
Data / restraints / parameters	7665 / 0 / 406	
Goodness-of-fit on F^2	1.031	
Final R indices [I>2sigma(I)]	R1 = 0.0373, wR2 = 0.0707	
R indices (all data)	R1 = 0.0810, wR2 = 0.0837	
Absolute structure parameter	-0.007(8)	
Extinction coefficient	n/a	
Largest diff. peak and hole	0.363 and -0.634 e.Å^{-3}	

References

1 M. V. Gradiski, B. T. H. Tsui, A. J. Lough and R. H. Morris, *Dalton Trans.*, 2019, **48**, 2150–2159.
2 T. Rodima, I. Kaljurand, A. Pihl, V. Mäemets, I. Leito and I. A. Koppel, *J. Org. Chem.*, 2002, **67**, 1873–1881.
3 C. F. Wise, R. G. Agarwal and J. M. Mayer, *J. Am. Chem. Soc.*, 2020, **142**, 10681–10691.